

Stephen F. Austin State University

SFA ScholarWorks

Electronic Theses and Dissertations

5-2020

Synthesis and Characterization of Carbon Monoxide Producers Bipyridine Flavonolate Palladium(II) and Platinum(II) Complexes: Potential Anti-Cancer Agents

Sarah Whitfield

Stephen F Austin State University, dgwhitfield@hotmail.com

Follow this and additional works at: <https://scholarworks.sfasu.edu/etds>

 Part of the [Inorganic Chemistry Commons](#)

[Tell us](#) how this article helped you.

Repository Citation

Whitfield, Sarah, "Synthesis and Characterization of Carbon Monoxide Producers Bipyridine Flavonolate Palladium(II) and Platinum(II) Complexes: Potential Anti-Cancer Agents" (2020). *Electronic Theses and Dissertations*. 291.

<https://scholarworks.sfasu.edu/etds/291>

This Thesis is brought to you for free and open access by SFA ScholarWorks. It has been accepted for inclusion in Electronic Theses and Dissertations by an authorized administrator of SFA ScholarWorks. For more information, please contact cdsscholarworks@sfasu.edu.

Synthesis and Characterization of Carbon Monoxide Producers Bipyridine Flavonolate Palladium(II) and Platinum(II) Complexes: Potential Anti-Cancer Agents

Creative Commons License



This work is licensed under a [Creative Commons Attribution-Noncommercial-No Derivative Works 4.0 License](https://creativecommons.org/licenses/by-nc-nd/4.0/).

Synthesis and Characterization of Carbon Monoxide Producers Bipyridine Flavonolate
Palladium(II) and Platinum(II) Complexes: Potential Anti-Cancer Agents

By

SARAH L. WHITFIELD

B.S. in Secondary Education; B.A. in Chemistry, Texas A&M University

Presented to the Faculty of the Graduate School of Stephen F. Austin State University

In Partial Fulfillment

Of the Requirements

For the Degree of

Master of Science in Natural Science with a Concentration in Chemistry

STEPHEN F. AUSTIN STATE UNIVERSITY

May 2020

Synthesis and Characterization of Carbon Monoxide Producers Bipyridine Flavonolate
Palladium(II) and Platinum(II) Complexes: Potential Anti-Cancer Agents

By

SARAH L. WHITFIELD

B.S. in Secondary Education; B.A. in Chemistry, Texas A&M University

APPROVED:

Xiaozhen Han, Ph.D., Thesis Director

J. Brannon Gary, Ph.D., Committee Member

Michele Harris, Ph.D., Committee Member

Robert Wiggers, Ph.D., Committee Member

Matibur Zamadar, Ph.D., Committee Member

Pauline M. Sampson, Ph.D.
Dean of Research and Graduate Studies

ABSTRACT

Novel designed metal ligand complexes as prodrugs are useful in the effort to find more effective and selective anti-cancer treatments. Carbon monoxide, CO, is known to induce mitochondrial collapse in cancer cells. Herein is described the synthesis of seven novel bipyridine flavonolate palladium(II) and platinum(II) complexes with the property of releasing carbon monoxide, and their characterization with FTIR, UV-Vis, fluorescence, NMR, and ESI mass spectra. Their ability to release carbon monoxide was investigated through oxygenation reaction under various conditions of temperature and light irradiation. The nitroxygenation reaction of the palladium complexes was also studied with nitrosyl hydride, HNO, generated in situ from Angeli's salt. Deoxymyoglobin was used to trap CO released from the complexes, and the reaction was monitored spectroscopically. The spectra showed that oxygenation reaction did not produce CO in the palladium complexes but did in the platinum complexes with irradiation, whereas nitroxygenation reaction did in the palladium complexes.

ACKNOWLEDGEMENTS

I would like to express appreciation to my research advisor Dr. Xiaozhen Han and to Dr. Michael A. Janusa, Chair/Professor of Chemistry and Biochemistry at SFASU. I would also like to thank the Baylor University Department of Chemistry for the high resolution mass spectra. The Texas Academy of Science and the Welch Foundation Departmental Grant (AN-0008) graciously provided support for this research. Finally, I would like to thank fellow members of Dr. Han's research team, Jacob Cotten and Ivan Jimenez.

TABLE OF CONTENTS

ABSTRACT	iii
ACKNOWLEDGEMENTS	iv
LIST OF FIGURES	vii
LIST OF TABLES	xii
LIST OF SCHEMES.....	xiii
CHAPTER 1 - INTRODUCTION.....	1
1.1 Flavonols	3
1.1a Structure of Flavonols.....	3
1.1b Function of Flavonols.....	4
1.1c CO-Release in Flavonols	6
1.2 Metalloflavonolato Complexes	9
1.2a Structure of Metalloflavonolato Complexes.....	9
1.2b Function of Metalloflavonolato Complexes	10
CHAPTER 2 - MATERIALS AND METHODS	14
2.1 General procedure for preparation of 1-4	15
2.2 General Procedure for Preparation of 5-7	15
2.3 Reaction of 3 and O ₂	19

2.4 Reaction with O ₂ under light.....	19
2.5 Reaction of 1-4 and HNO.....	19
2.6 Detection of photo-induced CO release	20
CHAPTER 3 - RESULTS AND DISCUSSION	21
3.1 Synthesis and characterization of Pd(II) and Pt(II) flavonolate complexes.....	21
3.2 Spectroscopic properties of the complexes	21
3.3 ESI-MS Spectrometry	31
3.4 NMR spectroscopy	38
3.5 Oxygenation of Pd(II) bipyridine flavonolate complexes with O ₂	45
3.6 Oxygenation of Pt(II) bipyridine flavonolate complexes with O ₂	48
3.7 Nitroxxygenation of Pd(II) bipyridine flavonolate complexes with HNO	51
3.8 CO detection from nitroxxygenation reaction of [PdBpyFla]BF ₄ with HNO.....	55
CHAPTER 4 - CONCLUSIONS	58
REFERENCES	60
VITA.....	67

LIST OF FIGURES

Figure 1. Basic structure of a 3-hydroxyflavonol.	3
Figure 2. Structure of (A) a synthetic 3-O-aminoalkyl-3',4'-O-dimethoxyflavonol, (B) myricetin (C) TMFol,	4
Figure 3. One proposed mechanism of CO release.....	8
Figure 4. CORM-S1, a visible-light-activated photoCORM.	12
Figure 5. FTIR spectrum of complex 5	23
Figure 6. FTIR spectrum of complex 6	23
Figure 7. FTIR spectrum of complex 7	24
Figure 8. UV-Vis spectrum of complex 1 (50 μ M in acetonitrile)	25
Figure 9. UV-Vis spectrum of complex 2 (50 μ M in acetonitrile).	25
Figure 10. UV-Vis spectrum of complex 3 (50 μ M in acetonitrile)	26
Figure 11. UV-Vis spectrum of complex 4 (50 μ M in acetonitrile).	26
Figure 12. UV-Vis spectrum of complex 5 (25 μ M in DMSO).....	27
Figure 13. UV-Vis spectrum of complex 6 (25 μ M in DMSO).....	27

Figure 14. UV-Vis spectrum of complex 7 (25 μM in DMSO).....	28
Figure 15. (a) UV-Vis spectrum of complex 3 (50 μM in acetonitrile, solid line) and product after reacting with O_2 in acetonitrile at 80°C (dashed line). (b) Plot of λ_{max} of the complexes vs. Hammett constant σ for complexes 1-4	29
Figure 16. Plot of λ_{max} of the complexes vs. Hammett constant σ for complexes 5-7	29
Figure 17. Fluorescence spectrum of complex 5	30
Figure 18. Fluorescence spectrum of complex 6	30
Figure 19. Fluorescence spectrum of complex 7	31
Figure 20. (a) Zoomed blank mass spectrum before sample. (b) Zoomed isotope pattern on mass spectrum of complex 1 . (c) Zoomed theoretical isotope distribution of complex 1	32
Figure 21. (a) Zoomed blank mass spectrum before sample. (b) Zoomed isotope pattern on mass spectrum of complex 2 . (c) Zoomed theoretical isotope distribution of complex 2	33
Figure 22. (a) Zoomed blank mass spectrum before sample. (b) Zoomed isotope pattern on mass spectrum of complex 3 . (c) Zoomed theoretical isotope distribution of complex 3	34
Figure 23. (a) Zoomed blank mass spectrum before sample. (b) Zoomed isotope pattern on mass spectrum of complex 4 . (c) Zoomed theoretical isotope distribution of complex 4	35
Figure 24. (a) Zoomed blank mass spectrum before sample. (b) Zoomed isotope pattern on mass spectrum of complex 5 . (c) Zoomed theoretical isotope distribution of complex 5	36

Figure 25. (a) Zoomed blank mass spectrum before sample. (b) Zoomed isotope pattern on mass spectrum of complex 6 . (c) Zoomed theoretical isotope distribution of complex 6	37
Figure 26. (a) Zoomed blank mass spectrum before sample. (b) Zoomed isotope pattern on mass spectrum of complex 7 . (c) Zoomed theoretical isotope distribution of complex 7	38
Figure 27. ^1H NMR spectrum of complex 3	39
Figure 28. ^{13}C NMR spectrum of complex 3	40
Figure 29. 2D ^1H - ^1H COSY of complex 3	40
Figure 30. 2D ^{13}C - ^1H HSQC of complex 3	41
Figure 31. 2D ^{13}C - ^1H HMBC of complex 3	41
Figure 32. ^1H NMR spectrum of complex 1	42
Figure 33. ^1H NMR spectrum of complex 2	42
Figure 34. ^1H NMR spectrum of complex 4	43
Figure 35. ^1H NMR spectrum of complex 5 in CD_3CN	43
Figure 36. ^1H NMR spectrum of complex 6 in CD_3CN	44
Figure 37. ^1H NMR spectrum of complex 7 in CD_3CN	44
Figure 38. ^{13}C NMR spectrum of complex 7 in $(\text{CD}_3)_2\text{SO}$	45

Figure 39. UV-Vis absorption spectra of reaction between complex 1 and O ₂ with light irradiation under Ar in acetonitrile.	46
Figure 40. UV-Vis absorption spectra of reaction between complex 2 and O ₂ with light irradiation under Ar in acetonitrile.	47
Figure 41. UV-Vis absorption spectra of reaction between complex 3 and O ₂ with light irradiation under Ar in acetonitrile.	47
Figure 42. UV-Vis absorption spectra of reaction between complex 4 and O ₂ with light irradiation under Ar in acetonitrile.	48
Figure 43. UV-Vis absorption spectra of reaction between complex 5 (25 μM) in DMSO and O ₂ with light irradiation at ambient temperature.	49
Figure 44. UV-Vis absorption spectra of reaction between complex 6 (25 μM) in DMSO and O ₂ with light irradiation at ambient temperature.	49
Figure 45. UV-Vis absorption spectra of reaction between complex 7 (25 μM) in DMSO and O ₂ with light irradiation at ambient temperature.	50
Figure 46. UV-Vis absorption spectra of reaction between complex 1 with HNO donor Angeli's salt in pH 7.1 phosphate buffer.	53
Figure 47. UV-Vis absorption spectra of reaction between complex 2 with HNO donor Angeli's salt in pH 7.1 phosphate buffer.	53
Figure 48. UV-Vis absorption spectra of reaction between complex 3 with HNO donor Angeli's salt in pH 7.1 phosphate buffer.	54
Figure 49. UV-Vis absorption spectra of reaction between complex 4 with HNO donor Angeli's salt in pH 7.1 phosphate buffer.	54

Figure 50. UV-Vis absorption spectra of reaction between complex **3** and NaNO_2 under Ar in acetonitrile. 55

Figure 51. UV-Vis spectra of formation of $\text{CO-Fe}^{\text{II}}\text{Mb}$ (dashed line) by deoxy-myoglobin trapping of CO released in the reaction of complex **3** with Angeli's salt. 56

LIST OF TABLES

Table 1. Summary of Infrared (IR) and Ultraviolet-Visible (UV-Vis) Data for Pd(II) and Pt(II) bipyridine flavonolate complexes.....	22
--	----

LIST OF SCHEMES

- Scheme 1:** Reaction of photoCORM, serum albumin and thiols to release CO.....7
- Scheme 2.** Proposed mechanism to release CO upon nitrooxygenation.....57
- Scheme 3.** Proposed mechanism to release CO upon oxygenation.....57

CHAPTER 1 - INTRODUCTION

Cancer is a disease characterized by frequent cell division, lack of regulated cell death, angiogenesis and increased glycolysis.¹ Direct medical expenses of cancer cost Americans an estimated \$80.2 billion in 2015 according to the Agency for Healthcare Research and Quality (AHRQ).² Current anticancer drugs face limitations such as development of drug resistance, lack of selectivity, and low efficacy.³ The medical community needs new cancer treatments.

Effectively fighting cancer requires a multi-faceted approach, perhaps combining treatments like radiotherapy, hormone therapy, chemotherapy and immunotherapy. Rather than targeting the cancer cells directly, immunotherapy attempts to activate and boost natural anti-cancer immune responses with therapies such as cancer vaccines³ and targeting immune system checkpoint inhibitors.⁴ Although immunotherapy is very promising, even the most successful immunotherapies induce adverse side effects in 60-75% of the patients.³⁻⁵ Immune checkpoint inhibitors can cause widespread inflammation, resulting in diseases like diabetes, hepatitis, or tuberculosis depending on which organ becomes inflamed.⁶ More research is needed to better understand the effective combinations and durations of therapies³ and to predict which patients are likely to have a serious reaction.⁷

Chemotherapy drugs can work through various means, such as inducing apoptosis (programmed cell death), interfering with cell proliferation, inhibiting angiogenesis (creation of new blood vessels that would encourage tumor growth), and interrupting metastasis (the spread of cancer to other parts of the body).⁸ Ideally a chemotherapy drug recognizes the target cancer cell and interacts with it in multiple ways,^{3,9} even in the hypoxic (low-oxygen) environment typically found in cancer cells.¹⁰ It must have adequate aqueous solubility but not undesired side reactions.¹¹

A prodrug (substance that undergoes a reaction during uptake and transport inside the body¹¹) that releases carbon monoxide could be an effective new chemotherapy. Despite its reputation as a noxious gas, carbon monoxide (CO) is a gaseous signaling molecule in the body, naturally regulating inflammatory mediators. As an anti-inflammatory agent, it gives cytoprotection to healthy cells.^{12,13} CO is beneficial in slowing the proliferation of some cancers by limiting angiogenesis activated by reactive oxygen species (ROS). Tumors characteristically overproduce ROS.¹⁴⁻¹⁶ CO targets the cancer cell's mitochondria by accelerating oxidative metabolism and inducing mitochondrial collapse.^{12,14} It can even amplify the effectiveness of other chemotherapy drugs used in combination with it.¹⁴ One study showed that murine prostate cancer treated with low concentrations of carbon monoxide followed by the chemotherapy agent camptothecin amplified the effect of the drug 1000-fold.¹⁴ This drug sensitization of only cancer cells but not normal cells means lower doses could be used, resulting in fewer adverse side effects and less chance of developing drug resistance.

The objectives pursued in this thesis are to synthesize novel bipyridine platinum and palladium flavonolate complexes and to determine their photo-induced carbon monoxide release as potential anticancer agents. The research includes characterizing these novel complexes by FTIR spectroscopy, UV-Vis spectroscopy, fluorescence spectroscopy, ESI high resolution mass spectrometry, ^1H and ^{13}C NMR spectroscopy and elemental analysis.

1.1 Flavonols

1.1a Structure of Flavonols

Flavonols, a subclass of flavonoids, can produce carbon monoxide molecules. About 200 flavonols have been identified in vegetables and fruits such as kale, broccoli, cranberries, blueberries and citrus fruit.^{17,18} As seen in Figure 1, flavonols are made of two benzene rings connected by a pyrone ring, an unsaturated O-heterocyclic ring with a ketone functional group.^{17,19,20}

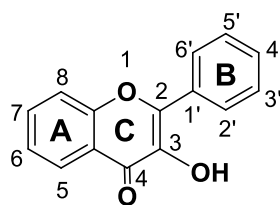


Figure 1. Basic structure of a 3-hydroxyflavonol.

Flavonols are amphipathic in that the phenolic hydroxyl substituents are hydrophilic, and the benzene rings are hydrophobic. This amphipathic nature can be advantageous to

increase aqueous solubility and promote interaction between the flavonol as a therapeutic agent and its biological target.^{21,22}

1.1b Function of Flavonols

Free flavonols have anti-inflammatory, antiviral, antifungal, antibacterial, anti-allergy, anti-diabetic, antiatherosclerotic, antithrombotic, hypolipidemic, anti-mutagenic, and anticancer properties.^{3,15,17,21–23} Their healthful benefits are tied to their ability to act as free radical scavengers.²⁴ 3-Hydroxyflavones (which have a hydroxyl group at C-3 of ring C) have particularly shown promise as anticancer agents.^{3,23,25–27} The most widely studied²² flavonol, quercetin, found in tea, apple, and onion,²⁸ exemplifies flavonols' antiproliferative properties toward meningioma cells and colon cancer cells at 10 μ M concentrations.²⁶ One study reports a 292-fold increase in potency against in vitro prostate cancer when the 3-hydroxy group on the C-ring was replaced by a dibutylamino group through a 3- to 5-carbon linker and the B ring included a catechol group. (Figure 2A).²⁷

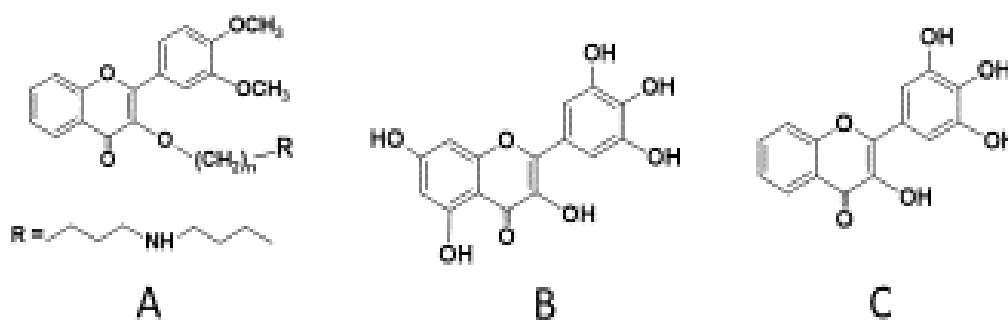


Figure 2. Structure of (A) a synthetic 3-O-aminoalkyl-3',4'-O-dimethoxyflavonol, (B) myricetin (C) TMFol,

Naturally-occurring myricetin, a 3',4',5'-hydroxyflavonol, (Figure **2B**) inhibits prostate cancer cell growth with $IC_{50} \leq 15 \mu\text{M}$.^{1,28} Additional hydroxy groups on the phenolic ring of the flavonol can increase the complex's antiproliferative ability due to the hydroxylated aromatic structure.¹⁷ However, the hydroxy groups can also promote pro-oxidant activity by reducing Cu^{II} to Cu^{I} or Fe^{III} to Fe^{II} or by auto-oxidizing in alkaline media to generate ROS like superoxide anions.²² This occurs particularly when the B ring has three or more hydroxyl substituents.¹⁷ This paradox of being simultaneously pro-oxidant and anti-oxidant is consistent with the observation that many anticancer agents also have carcinogenic potential.¹ Likewise, the generation of ROS can have a positive effect on cancer therapy but a negative effect on chemoprevention.

Flavonols additionally inhibit signal transduction pathways and other growth regulatory pathways in the cell.^{1,22} For example, they inhibit topoisomerase $\text{II}\alpha$, an enzyme overexpressed in many types of cancer^{9,19} and whose inhibition interferes with DNA replication.^{1,3,9,25,29,30} Flavonols also inhibit kinases which are involved in cell metabolism.^{1,3,9,25,26,29,30} Having a catechol group at 3'- and 4'-positions on the B ring confers maximum inhibition of kinases.²⁶ Several flavonol analogues inhibit cell growth and expression of androgen receptor and/or prostate specific antigen (PSA) in prostate cancer.²⁸

Flavonols work synergistically with other treatments.¹ For example, the flavonol isorhamnetin protects against cardiotoxicity induced by the platinum-based drug

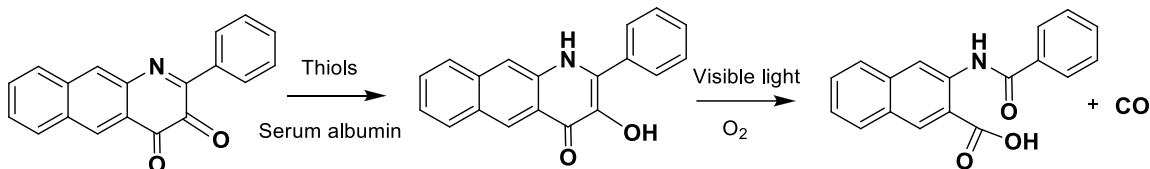
doxorubicin in vivo.¹ A quercetin derivative inhibits multiple drug resistance in breast cancer.¹

A synthetic 3',4',5'-trimethoxyflavonol complex analogous to myricetin, TMFol, (Figure 2C) inhibits growth at even lower IC₅₀ values. This may be because its methoxy (OMe) groups' antioxidant activity is not reduced by hydrogen bonding between ligand and solvent molecules as seen with myricetin's hydroxyl ligands.¹⁷ Additionally, methoxyl groups make the complex less polar than hydroxyl groups, so the molecule is more permeable to biological membranes.²⁶

1.1c CO-Release in Flavonols

In addition to their other anti-cancer properties, flavonols could treat cancer by releasing carbon monoxide upon photo-irradiation in the presence of dioxygen.^{12,18,29,31-34} These visible-light-activated carbon-monoxide-releasing molecules (photoCORMS) provide a newer method to control the release of CO. They use visible light to trigger the release of a small amount of carbon monoxide to a very specific target with less harm to healthy cells. Visible light activation is preferred over UV-light activation since the latter has poorer penetration and can possibly harm healthy tissue.¹³ Berreau et al. developed a prodrug photoCORM in which the carbon monoxide molecule is released from a flavone.³¹ Since the flavone photoCORMs have a high affinity for serum albumin, they are less likely to release CO until the albumin has carried the oxidized form of a photoCORM to the cancer cell. There it is reduced by biological thiols which are present in higher concentrations in

cancer cells (Scheme 1).³⁵ This mechanism means the CO is less likely to be released before reaching the target. In addition to the anticancer benefits, the Berreau study noted anti-inflammatory benefits of the photoCORM at nanomolar concentrations.³¹



Scheme 1. Reaction of photoCORM, serum albumin and thiols to release CO.

A 2017 study proposes a delivery system to release the carbon monoxide only after it reaches the target cancer cell.³² It employs a “sense-of-logic carbon monoxide-releasing molecule” (SL-photo-CORM) that requires two triggers to release CO. A flavonol reacts with acryloyl chloride to produce an SL-photo-CORM. The first trigger is thiol sensing. When the photoCORM senses biological thiols, the reverse reaction occurs creating an activated flavonol molecule. The second trigger is visible light. When the activated flavonol senses visible light in the presence of dioxygen, it releases a carbon monoxide molecule and produces a non-fluorescing, nontoxic product. The reaction will occur even in the reduced-oxygen environment typically found in cancer cells.

Several studies have focused on how carbon monoxide is released from the flavonol.^{33,36,37} Natural enzymes like quercetin dioxygenase cleave the C ring of the flavonol in a 1,3-*endo*-peroxide pathway to release CO.^{33,36} A DFT study³⁶ proposes that the Cu^{II} metal center of the enzyme binds to the flavonol, then the copper is reduced in a

single electron transfer (SET) as dioxygen attacks the flavonol to form a flavonol radical with a bridging peroxide structure, as shown in Figure 3. After this, the O-O bond and a C-C bond cleave concertedly to release the carbon monoxide molecule.

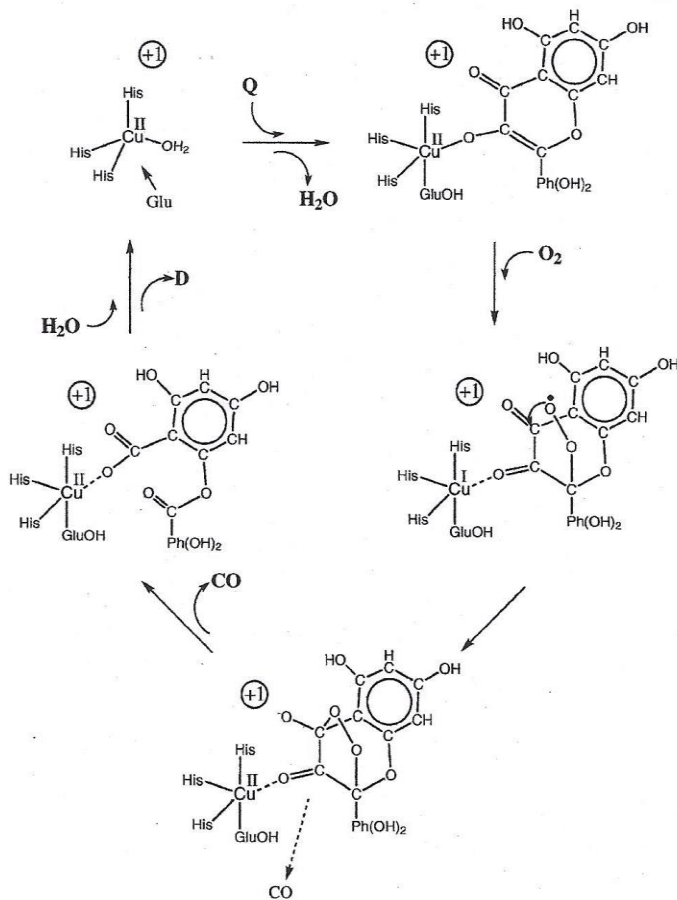


Figure 3. One proposed mechanism of CO release.³⁶

1.2 Metalloflavonolato Complexes

1.2a Structure of Metalloflavonolato Complexes

Many researchers are taking advantage of the multiple coordination sites on transition metals to design drugs with ligands that have anticancer properties,¹¹ particularly flavonols.²² Hydroxyflavones form stable coordination complexes with bidentate binding at the hydroxyl and carbonyl groups of ring C.^{17,22} Flavonols may also bind to the metal between the 5-hydroxy (ring A) and 4-carbonyl (ring C) groups or between 3'- and 4'-hydroxy groups in ring B, although both of these chelations are significantly less favorable thermodynamically than 3-hydroxy/4-carbonyl coordination.^{17,20,21} Due to its proximity to the carbonyl group, the 3-hydroxyl proton on ring C is more acidic than the hydroxyl protons on rings A and B. In the coordinate bond the 3-hydroxyl oxygen electrons are delocalized which consequently increases delocalization of the π electrons.¹⁷ Thus the 3-hydroxyl chelation is more stable than the other hydroxyl chelation sites. Metal-flavonolates typically bind in a 1:1 metal:ligand (M:L) ratio but can bind in a 1:2 (M:L) ratio with additional chelation involving *ortho* hydroxy groups on the B ring.^{17,22} The ideal pH for complexation for most metals is pH 9.5 because this facilitates deprotonation of the hydroxy groups to activate the flavonol.¹⁷

Steric effects of substituents on the flavonol are very influential on the anticancer efficacy. Bulky flavonols cause steric hindrance to the metal-flavonol chelation.²² The electronic effects of substituents on the flavonolate ligand have also been studied. For example, the hydroxy groups have been substituted with electron withdrawing groups and

electron donating groups such as methoxyl, thionyl, and acetamide groups.¹⁹ The electronic effects of these substituents appear to have only a minor effect on the cytotoxicity of the complexes.

1.2b Function of Metalloflavonolato Complexes

Flavonol's biological properties usually improve when the flavonol coordinates with a metal. For example, the natural flavonol quercetin coordinated with zinc or manganese exhibits greater anti-inflammatory properties than quercetin alone.²² Lanthanide-quercetin complexes exhibit greater antitumor properties than free quercetin.²² The enhanced anti-cancer properties come from the metal binding to the cancer cell's DNA to induce apoptosis,^{10,29,30,38} combined with the anti-cancer activity of the flavonol. Also, flavonols' solubility is improved four-fold¹⁹ or ten-fold³⁹ when coordinated to a metal complex rather than in unbound form. Bioavailability increases as solubility increases. Coordination also decreases the possibility of the flavonol being metabolized to an inactive form.^{1,27} The superior anticancer properties of flavonolate complexes compared to free flavonols are also due to a reduction in the metal's redox potential so it is less likely to form radicals.²² In addition to this aspect of flavonolate complexes acting as antioxidants, flavonols also directly neutralize reactive oxygen species and inhibit enzymes that catalyze processes which generate ROS.¹⁷

Another explanation for chelated flavonols' stronger anticancer activity compared to free flavonols is that coordination complexes such as ruthenium-(3-hydroxyflavone)

generally are more lipophilic than the free flavonols. This permits higher accumulation in the cancer cell. Nevertheless, there is not a clear relationship between lipophilicity and cytotoxicity. For example, 3',5'-dimethoxyflavone is more cytotoxic than 3',4'-dimethoxyflavone, but the more lipophilic 3',4',5'-trimethoxyflavone is less cytotoxic.¹⁹ The position of substitutions on the phenyl ring seems to be more influential on cytotoxicity than lipophilicity, perhaps due to varying amounts of twisting the ring out of plane and therefore changing interaction with the biological target.^{9,19,20} *Ortho* substituents on the B ring showed the lowest cytotoxicity, with a torsion angle of 60.22° seen in an *o*-difluoro-substituted phenyl ring.^{19,39} Ru^{II}(η^6 -*p*-cymene) complexes with *para*-chloro substituents formed the strongest anticancer complexes.⁹

One significant benefit of releasing carbon monoxide from a metal-flavonolate complex is controlled release of the CO. Controlled release is an important consideration when using carbon monoxide as an anticancer agent. It is easier to control the release of CO from the flavonolate ligand in a dioxygenase-type reaction than from the carbonyl in a dissociative reaction from the metal.^{13,31} Metal carbonyl photoCORMs sometimes leak, that is, spontaneously release CO before arriving at their target.³¹ The chance of premature release of CO means higher concentrations of the photoCORM are needed to deliver a toxic dose to the cancer cells with consequently increased risk to healthy cells. CO release from the complexes can be controlled through choice of ancillary ligands.¹³ By selecting π -donor ancillary ligands that increase the hyperconjugation of the complex, the HOMO-LUMO energy gap between the metal's d-orbitals and the CO's π^* molecular orbitals can be

reduced to the range of visible light. The putative first visible-light-activated photoCORM was a dicarbonylbis(cysteamine)iron(II) complex (Figure 4) that released CO at 470nm light irradiation.¹³

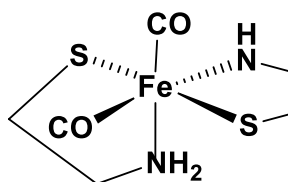


Figure 4. CORM-S1, a visible-light-activated photoCORM.

Well-chosen ancillary ligands can also improve solubility/bioavailability of the complex. Ancillary ligands can ensure that the byproducts of CO release are non-toxic and easily eliminated from the body.¹³

Carbon monoxide release in metal-flavonolate complexes can follow two different pathways. One photooxygenation pathway involves a diradical intermediate that reacts with triplet dioxygen (a diradical in the ground state). A second pathway involves a single electron transfer from the O-heterocycle to dioxygen resulting in a tautomer of the diradical and a superoxide ion.³³ In either case, a bridging peroxide forms, followed by a concerted C-C bond cleavage and O-O peroxide bond cleavage to release CO. The reaction without an enzyme typically requires either UV light or visible light with high temperatures (70°C - 80°C).³³ The wavelength of light used in the photoinduced oxygenation gives different products: UV light (300 nm) yields a 1,3 addition product, but visible light (400nm) yields

a 1,2 addition product.^{29,33} One study found that UV light yielded 0.7 equivalents of free CO whereas visible light yielded only 0.4 equivalents.²⁹

Many different flavonolate coordination complexes have been created, including ones with ruthenium(II), iron(II), zinc(II), copper(II), lead(II), aluminum(III), tin(II), cadmium(II), cobalt(II), osmium(II), and rhodium(II).^{17,19} Nevertheless, despite variations in properties of these metal complexes, the anticancer effects are mainly due to bioactivity of the O,O-chelating flavonolates ligands, rather than the choice of metal.^{25,39}

Flavonols are promising ligands in a coordination complex because they work in multiple ways to fight a diversity of cancer types such as bladder, breast, colon and thyroid cancers.^{1,11} Bipyridine metal flavonolate complexes could provide a novel way for an anticancer agent to deliver small amounts of carbon monoxide selectively to the cancer cells. If the carbon monoxide efficiently targets the cancer cell, then a lower dose of the drug would be possible, with fewer side effects and less chance of developing drug resistance. The flavonolate complexes may contribute additional anticancer effects, such as attacking cancer DNA, scavenging reactive oxygen species, and inhibiting enzymes to stop cancer cell proliferation.

CHAPTER 2 - MATERIALS AND METHODS

All reagents and solvents were obtained from commercial sources and were used as received. The (2,2'-bipyridine)dichloropalladium(II) ($\text{Pd}(\text{Bpy})\text{Cl}_2$), (2,2'-bipyridine)dichloroplatinum(II) ($\text{Pt}(\text{Bpy})\text{Cl}_2$), silver tetrafluoroborate (AgBF_4), 3-hydroxyflavone (Fla), 3-hydroxy-4'-methoxyflavone (Fla-OMe), Angeli's salt, and solvents were purchased from Sigma. The 3-hydroxy-4'-methylflavone (Fla-Me) and 3-hydroxy-4'-chloroflavone (Fla-Cl) were obtained from Otave. FTIR data was collected on a Perkin Elmer Spectrum 100 FTIR spectrometer. UV-Vis spectra were recorded at ambient temperature using an Agilent HP8453 diode array spectrophotometer in a standard UV-Vis quartz cuvette. Fluorescence data was collected on a Perkin Elmer FL6500 Fluorescence Spectrometer. High resolution mass spectra (HRMS) were obtained in the Baylor University Mass Spectrometry Center on a Thermo Scientific LTQ Orbitrap Discovery spectrometer using +ESI.⁴⁰ ^1H , ^{13}C , and 2D NMR spectra were obtained at ambient temperature in CD_3CN solution for the palladium complexes and in $(\text{CD}_3)_2\text{SO}$ for the platinum complexes, both on a Jeol ECS 400 MHz NMR spectrometer. J values are given in Hz. A Rayonet Photochemical Reactor, RPR-100, equipped with RPR-5750A lamps was used for all photochemical reactions. CO was detected using myoglobin assay according to literature procedures.

2.1 General procedure for preparation of **1-4**

Silver tetrafluoroborate (AgBF_4) (0.6 mmol) was dissolved in methanol (7 mL); (2,2'-bipyridine)dichloropalladium(II) ($\text{Pd}(\text{Bpy})\text{Cl}_2$) (0.3 mmol) was dissolved in DMSO (1 mL), and then the solutions were stirred together at ambient temperature 0.5 h. Following gravity filtration, solid 3-hydroxyflavone derivative (0.3 mmol) and triethylamine (0.7 mL) were added to the filtrate. The reaction mixture was stirred for 0.25 h (2 h for the Fla-OMe) at ambient temperature. The corresponding bipyridine palladium(II) flavonolato salt was then recovered using vacuum filtration and recrystallized in $\text{CH}_3\text{OH}/\text{CH}_3\text{CN}$ solvent; remaining solvent was removed in a vacuum desiccator overnight.

2.2 General Procedure for Preparation of **5-7**

Silver tetrafluoroborate (AgBF_4) (0.4 mmol) was dissolved in methanol (4 mL); (2,2'-bipyridine)dichloroplatinum(II) ($\text{Pt}^{\text{II}}(\text{Bpy})\text{Cl}_2$) (0.2 mmol) was dissolved in DMSO (4 mL), and then the solutions were stirred together at ambient temperature 1 h. Following gravity filtration, solid 3-hydroxyflavone derivative (0.2 mmol) and triethylamine (1 mL) were added to the filtrate. The reaction mixture was stirred for 6 h at ambient temperature. The corresponding bipyridine platinum(II) flavonolato salt was then recovered using vacuum filtration and recrystallized in $\text{CH}_3\text{OH}/\text{CH}_3\text{CN}$ solvent; remaining solvent was removed in a vacuum desiccator overnight.

[(Pd(Bpy)(3-Hydroxy-4'-methoxyfla)][PF₆] **Complex 1**. Yield: 70% (orange crystals)
UV-Vis λ_{max} ($\text{CH}_3\text{CN}/\text{nm}$)($\epsilon/\text{M}^{-1} \text{cm}^{-1}$) (444 (25 200)); $^1\text{H NMR}$ (CD_3CN , 400 MHz): δ 7.92

(d, $J = 6.5$ Hz, 2H), 7.85 (m, $J = 21.9$ Hz, 4H), 7.65 (t, $J = 18.7$, 2H), 7.47 (d, $J = 7.3$ Hz, 2H), 7.28 (t, $J = 11.4$ Hz, 1 H), 7.19 (d, $J = 6.5$ Hz, 2 H), 7.13 (t, $J = 13.9$ Hz, 1 H), 6.66 (d, $J = 8.1$ Hz, 2 H); ^{13}C NMR (CD_3CN , 400 MHz): $\delta = 181.44, 161.13, 153.96, 153.65, 152.62, 151.82, 150.65, 148.54, 148.20, 140.94, 140.67, 138.01, 133.05, 129.37, 129.14, 127.34, 127.27, 125.04, 124.44, 124.03, 123.10, 123.01, 121.96, 121.73, 117.45, 115.53, 54.91$ ppm. +ESI-MS m/z (100%) calc. 529.04; found: 529.04. Elemental analysis calc. for $\text{C}_{26}\text{H}_{19}\text{BF}_4\text{N}_2\text{O}_4\text{Pd}$: C 50.64%, H 3.11%, N 4.54%; found: C 50.51%, H 3.01%, N 4.52%.

[(Pd(Bpy)(3-Hydroxy-4'-methylfla))][PF₆] **Complex 2.** Yield: 75% (light orange crystals) UV-Vis λ_{max} ($\text{CH}_3\text{CN}/\text{nm}$)($\epsilon/\text{M}^{-1} \text{cm}^{-1}$) 439 (22 200); ^1H NMR (CD_3CN , 400 MHz): δ 8.08 (d, $J = 5.5$ Hz, 1H), 8.03 (m, $J = 5.5$ Hz, 5H), 7.82 (t, $J = 15.7$ Hz, 2H), 7.70 (d, $J = 7.1$ Hz, 1H), 7.61 (t, $J = 14.9$ Hz, 1H), 7.43 (t, $J = 12.6$ Hz, 1H), 7.36 (m, $J = 19.6$ Hz, 2H), 7.27 (t, $J = 14.1$ Hz, 1H), 7.07 (d, $J = 7.1$ Hz, 2H); ^{13}C NMR (CD_3CN , 400 MHz): $\delta = 183.3, 155.2, 154.8, 154.0, 153.1, 151.3, 149.4, 142.2, 141.9, 134.5, 129.7, 128.5, 128.1, 127.6, 126.2, 124.3, 122.8, 119.3, 118.3, 40.93$ ppm. +ESI-MS m/z (100%) calc. 513.04; found: 513.04. Elemental analysis calc. for $\text{C}_{26}\text{H}_{19}\text{BF}_4\text{N}_2\text{O}_3\text{Pd}$: C 51.99%, H 3.19%, N 4.66%; found: C 51.51%, H 3.11%, N 4.62%.

[(Pd(Bpy)(3-Hydroxyfla))][PF₆] **Complex 3.** Yield: 80% (light orange crystals) UV-Vis λ_{max} ($\text{CH}_3\text{CN}/\text{nm}$)($\epsilon/\text{M}^{-1} \text{cm}^{-1}$) 434 (21 000); ^1H NMR (CD_3CN , 400 MHz): δ 8.06 (d, $J = 7.9$ Hz, 2H), 8.01 (d, $J = 5.5$ Hz, 1H), 7.91 (m, $J = 20.6$ Hz, 3H), 7.72 (t, $J = 10.3$ Hz, 2H), 7.64 (d, $J = 7.9$ Hz, 1 H), 7.59 (t, $J = 15.8$ Hz, 1 H), 7.35 (m, $J = 20.1$ Hz, 3 H), 7.29 (t, $J =$

15.2 Hz, 2 H), 7.22 (t, J = 13.3 Hz, 2 H); ^{13}C NMR (CD_3CN , 400 MHz): δ = 188, 154.8, 154.5, 153.0, 149.6, 149.0, 141.6, 141.0, 134.4, 131.4, 130.0, 128.8, 128.0, 127.8, 126.0, 123.4, 122.6 ppm. +ESI-MS m/z (100%) calc. 499.03; found: 499.02. Elemental analysis calc. for $\text{C}_{25}\text{H}_{17}\text{BF}_4\text{N}_2\text{O}_3\text{Pd}$: C 51.18%, H 2.92%, N 4.78%; found: C 51.11%, H 3.01%, N 4.72%.

[(Pd(Bpy)(3-Hydroxy-4'-chlorofla)][PF₆]] **Complex 4**. Yield: 84% (yellow crystals)
UV-Vis λ_{max} ($\text{CH}_3\text{CN}/\text{nm}$)($\epsilon/\text{M}^{-1}\text{cm}^{-1}$) 428 (20 400); ^1H NMR (CD_3CN , 400 MHz): δ 7.92 (m, J = 28.1 Hz, 2H), 7.80 (d, J = 7.5 Hz, 2H), 7.76 (d, J = 5.0 Hz, 1H), 7.69 (t, J = 16.3 Hz, 3H), 7.45 (t, J = 15.6 Hz, 1 H), 7.40 (d, J = 8.1 Hz, 1 H), 7.30 (t, J = 11.9 Hz, 1 H), 7.21 (t, J = 12.5 Hz, 1 H), 7.11 (d, J = 8.1 Hz., 1 H), 7.03 (m, J = 30.0 Hz, 3 H); ^{13}C NMR (CD_3CN , 400 MHz): δ = 184.0, 154.5, 154.3, 153.0, 149.5, 149.1, 141.8, 141.6, 136.5, 134.5, 129.1, 128.8, 128.1, 128.0, 125.9, 123.6, 122.5, 119.1 ppm. +ESI-MS m/z (100%) calc. 532.99; found: 532.99. Elemental analysis calc. for $\text{C}_{25}\text{H}_{16}\text{BClF}_4\text{N}_2\text{O}_3\text{Pd}$: C 48.35%, H 2.60%, N 4.51%; found: C 48.31%, H 2.65%, N 4.52%.

[(Pt(Bpy)(3-Hydroxy-4'-methoxyfla)][BF₄]] **Complex 5**. Yield: 70% (green crystals)
UV-Vis λ_{max} ($\text{CH}_3\text{CN}/\text{nm}$)($\epsilon/\text{M}^{-1}\text{cm}^{-1}$) (459 (33 000)); ^1H NMR (CD_3CN , 400 MHz): δ 8.35 (d, J = 4.5 Hz, 1H), 8.21 (d, J = 4.5 Hz, 1H), 8.06 (t, J = 16.6, 4H), 7.99 (d, J = 8.2 Hz, 2H), 7.69 (d, J = 8.5 Hz, 1 H), 7.62 (t, J = 15.4 Hz, 1H), 7.48 (t, J = 12.6 Hz, 1 H), 7.36 (d, J = 8.2 Hz, 2 H), 7.25 (t, J = 14.9 Hz, 1 H), 6.79 (d, J = 8.5 Hz, 2 H), 3.82 (s, 3H) ppm. +ESI-

HRMS m/z (relative intensity) calc. 618.30; found: 618.10. Elemental analysis calc. for $C_{26}H_{19}BF_4N_2O_4Pt$: C 44.28%, H 2.72%, N 3.97%; found: C 44.21%, H 2.75%, N 3.99%.

[(Pt(Bpy)(3-Hydroxy-4'-methylfla)][BF₄] Complex 6. Yield: 87% (green crystals) UV-Vis λ_{max} (CH₃CN/nm)($\epsilon/M^{-1} cm^{-1}$) (453 (25 000)); ¹H NMR (CD₃CN, 400 MHz): δ 8.46 (d, J = 4.8 Hz, 1H), 8.28 (d?, J = 4.7 Hz, 1H), 8.16 (t, J = 5.1, 4H), 7.99 (d, J = 7.6 Hz, 2H), 7.82 (d, J = 8.1 Hz, 1 H), 7.71 (t, J = 15.7 Hz, 1 H), 7.54 (m, J = 17.2 Hz, 1 H), 7.46 (d, J = 8.6 Hz, 1 H); 7.42 (t, J = 11.3 Hz, 1H), 7.34 (t, J = 14.5, 1H), 7.10 (d, J = 7.6 Hz, 2H), 3.30 (s, 3H) ppm. +ESI-HRMS m/z (relative intensity) calc. 602.31; found: 602.10. Elemental analysis calc. for $C_{26}H_{19}BF_4N_2O_3Pt$: C 45.30%, H 2.78%, N 4.06%; found: C 45.33%, H 2.76%, N 4.05%.

[(Pt(Bpy)(3-Hydroxyfla)][BF₄] Complex 7. Yield: 82% (green crystals) UV-Vis λ_{max} (CH₃CN/nm)($\epsilon/M^{-1} cm^{-1}$) (449 (11 000)); ¹H NMR (CD₃CN, 400 MHz): δ 8.81 (d, J = 5.4 Hz, 1H), 8.53 (d, J = 5.4 Hz, 1H), 8.34 (t, J = 6.8, 4H), 8.25 (m, J = 7.2 Hz, 2H), 8.11 (d, J = 4.1 Hz, 1 H), 7.84 (t, J = 7.8 Hz, 1 H), 7.73 (d, J = 4.5 Hz, 1 H), 7.67 (t, J = 6.5 Hz, 1 H), 7.54 (m, J = 8.5 Hz, 5H); ¹³C{¹H} NMR (CD₃CN, 400 MHz): δ = 184.5, 156.5, 156.4, 155.9, 155.2, 153.7, 152.5, 149.9, 141.8, 141.3, 135.1, 132.3, 130.3, 129.5, 129.0, 128.8, 127.1, 127.0, 124.8, 123.3, 118.9, 40.9 ppm. +ESI-HRMS m/z (relative intensity) calc. 588.29; found: 588.10. Elemental analysis calc. for $C_{25}H_{17}BF_4N_2O_3Pt$: C 44.47%, H 2.54%, N 4.15%; found: C 44.48%, H 2.50%, N 4.14%.

2.3 Reaction of **3** and O₂

A stock solution (35 μ L, 1.00 mM) of **3** in DMSO in an argon atmosphere was added to an inorganic phosphate (IP) buffer (2 mL, pH 7.1) in a screw-capped UV cuvette. Dioxygen was bubbled into it for 4 minutes. Carbon monoxide release was monitored by following the decrease of complex **3**'s absorbance at 434 nm for 1 h. The experiment was repeated using complexes **1**, **2** and **4** (100 μ L, 1.00 mM) at their corresponding λ_{max} . The experiment was also repeated at higher temperature (80 $^{\circ}$ C).

2.4 Reaction with O₂ under light

A stock solution (1.00 mM in DMSO) of **3** in an argon atmosphere was added to oxygen-saturated acetonitrile (2 mL) in a screw-capped UV cuvette. The cuvette was irradiated with broadband light and then monitored by UV-Vis spectroscopy in 10 s intervals three times, then 30 s intervals three times, then 1 min. intervals three times, then 3 minutes intervals for a total of 30 min.

A stock solution (25 μ M in DMSO) of **5** in an argon atmosphere was added to oxygen-saturated acetonitrile in a screw-capped UV cuvette. The cuvette was irradiated with broadband light then monitored by UV-Vis spectroscopy in 10 min. intervals for a total of 80 min. The experiment was repeated with complexes **6** and **7**.

2.5 Reaction of **1-4** and HNO

Because HNO is an analogue of dioxygen, the experiment was repeated using HNO. A buffered stock solution of the HNO-precursor Angeli's salt (AS) (10 mM, pH 12) was

prepared in an argon atmosphere according to literature procedures.⁴¹ AS (200 μ L, 10.00 mM) was added to an anaerobic flavonolato palladium stock solution (35 μ L, 1.00 mM) in IP buffer (2 mL, pH 7.1) in a screw-capped UV cuvette. The reaction was initiated by gently shaking the cuvette; carbon monoxide release was monitored by following the decrease of the substrate absorbance at 434 nm for 1 h. The experiment was repeated using complexes **1**, **2** and **4** (1.00 mM). Because NaOH is present in the IP buffer, a control reaction was run for NaOH (100 μ L, 0.1 M) reacting with complex **3** (35 μ L, 1.00 mM) in an argon atmosphere. Because sodium nitrite (NO_2^-) anions are a product of the decomposition of Angeli's salt, a control reaction was run for NO_2^- (100 μ L, 0.1 M) reacting with **3** (35 μ L, 1.00 mM). Both control reactions were monitored by absorption spectroscopy.

2.6 Detection of photo-induced CO release

Following literature procedures,¹⁶ argon was bubbled through complex **3** (4 μ mol) dissolved in DMSO (0.7 mL) and IP buffer (15 mL, pH 7.1) in a sealed round-bottom flask protected from light. Angeli's salt (10 mg) in an argon atmosphere was added and allowed to react. After 2h a sample of atmosphere from the head space was injected into a screw-capped UV cuvette containing an argon atmosphere with freshly prepared deoxymyoglobin (lyophilized horse skeletal muscle) (2 mL, 15 μ M) prepared by dissolving the protein in IP buffer (2 mL, 0.01M, pH 7.1) and reduced with sodium dithionite (90:1 molar ratio with myoglobin). The reaction was monitored spectroscopically.

CHAPTER 3 - RESULTS AND DISCUSSION

3.1 Synthesis and characterization of Pd(II) and Pt(II) flavonolate complexes

The synthesis of metal(II) bipyridine flavonolate complexes $[M^{II}BpyFla^R][BF_4]$ ($M = Pd$ (**1-4**), $R = p\text{-OMe}$ (**1**), $p\text{-Me}$ (**2**), $p\text{-H}$ (**3**), $p\text{-Cl}$ (**4**)); ($M = Pt$ (**5-7**), ($R = p\text{-OMe}$ (**5**), $p\text{-Me}$ (**6**), $p\text{-H}$ (**7**)) follows a methodology that has not been previously published. The complexes were prepared by mixing 1 equivalent of $M^{II}BpyCl_2$ with 2 equivalents of $AgBF_4$ first to generate activated $[M^{II}Bpy(sol)_2]$ moiety, followed by addition of 1.2 equivalents of deprotonated flavonol. The reaction was stirred under room temperature for 2 h (**1-4**) or 6 h (**5-7**). The resulting complexes were isolated as yellow-orange (**1-4**) or green (**5-7**) BF_4^- salts. The solid complexes **1-7** are stable in the air at room temperature for several months. The complexes have all been characterized by $^1H\text{-NMR}$, $^{13}C\text{-NMR}$, UV-Vis, infrared and fluorescence spectroscopies, and mass spectrometry, as well as elemental analysis.

3.2 Spectroscopic properties of the complexes

Pd^{II} - and Pt^{II} bipyridine flavonolate complexes (**1-7**) have very similar IR and electronic spectra as seen in **Table 1**.

Table 1. Summary of Infrared (IR) and Ultraviolet-Visible (UV-Vis) Data for Pd(II) and Pt(II) bipyridine flavonolate complexes.

Complex	λ_{\max} (nm)	Absorbance (AU)	Extinction Coefficient ϵ ($\text{cm}^{-1}\text{M}^{-1}$)	ν_{CO} (cm^{-1})	σ^a
1	444	1.26	2.52×10^4	1530	-0.27
2	439	1.11	2.22×10^4	1528	-0.17
3	434	1.05	2.10×10^4	1524	0
4	428	1.02	2.04×10^4	1520	0.23
5	459	0.815	3.3×10^4	1440	-0.27
6	453	0.628	2.5×10^4	1437	-0.17
7	449	0.527	1.1×10^4	1498	0

^a Hammett constants σ for substituents (OCH₃, CH₃, H and Cl)⁴²

Coordination of the flavonol to the metal site is indicated by the characteristic ν_{CO} band between 1450 and 1530 cm^{-1} (Figures **5-7**). Compared to that of the ν_{CO} vibration at 1602 cm^{-1} of the free flavonol, the band of complexes **1-4** is shifted by 70-80 cm^{-1} to lower energies and that of complexes **5-7** by 102-152 cm^{-1} , which can be explained by the formation of a stable five-membered chelate rings.^{18,43-51}

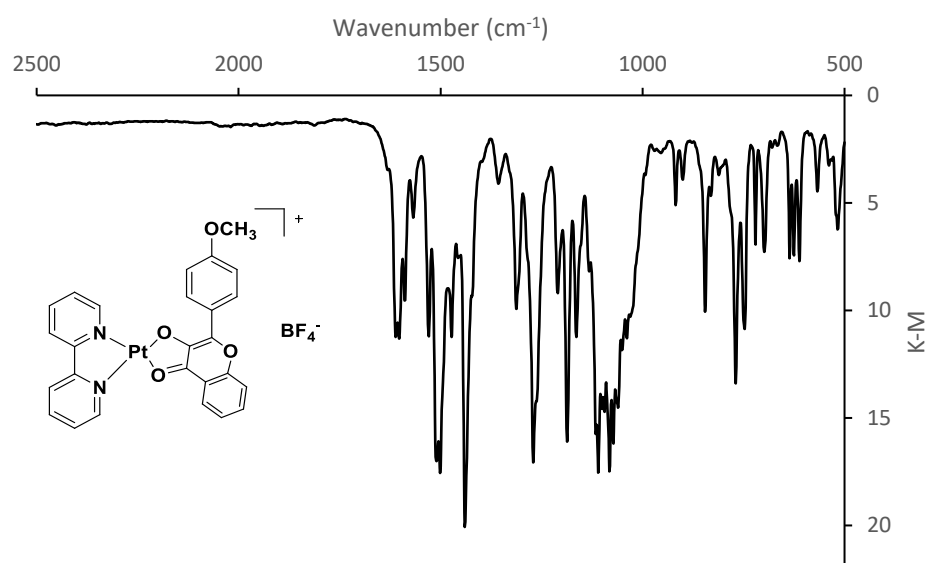


Figure 5. FTIR spectrum of complex 5.

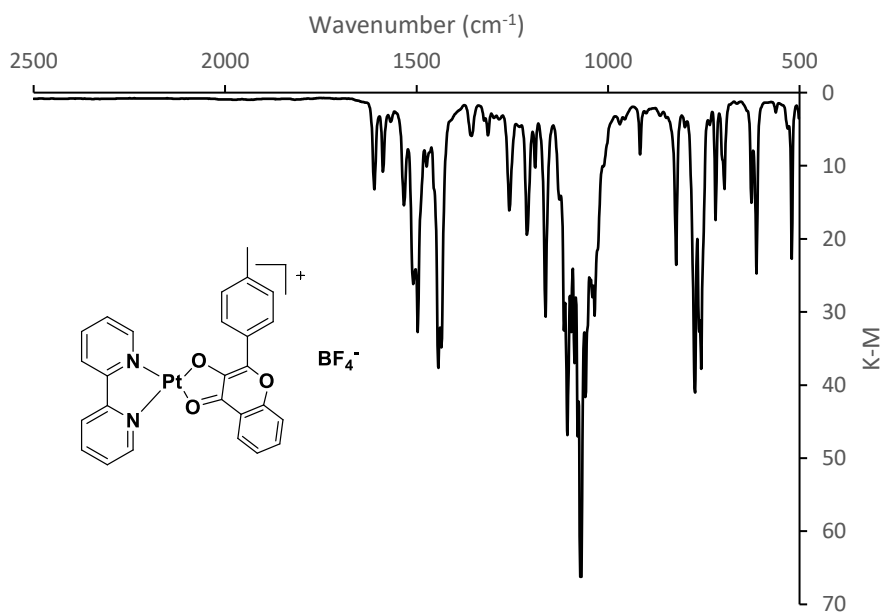


Figure 6. FTIR spectrum of complex 6.

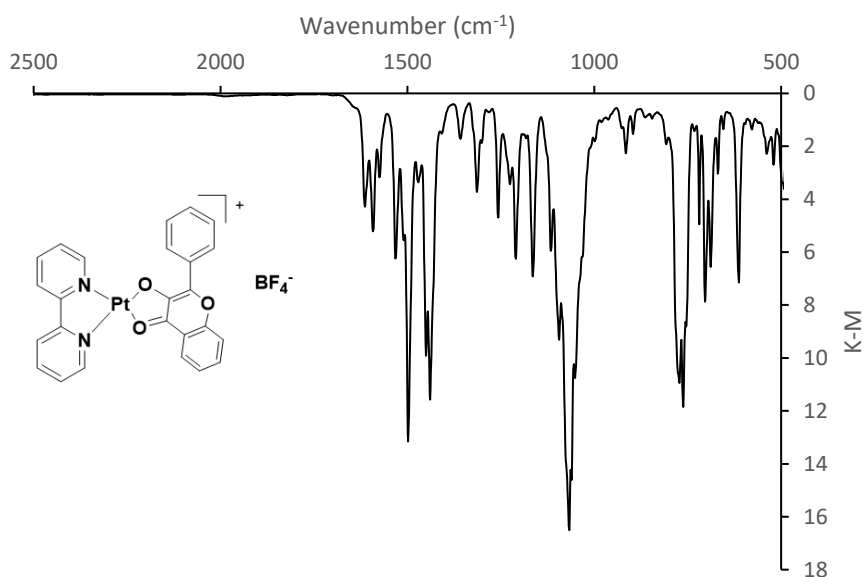


Figure 7. FTIR spectrum of complex **7**.

Neutral flavonol compounds exhibit an absorption feature in the range of 320-360 nm, which is assigned to the π - π^* transition (Figures **8-14**). When dissolved in CH_3CN under anaerobic conditions, each complex **1-4** exhibits an intense absorption feature in the range of 400–450 nm (complex **1**: 444 nm ($\epsilon = 2.5 \times 10^4 \text{ M}^{-1}\text{cm}^{-1}$), complex **2**: 439 nm ($\epsilon = 2.2 \times 10^4 \text{ M}^{-1}\text{cm}^{-1}$), complex **3**: 434 nm ($\epsilon = 2.1 \times 10^4 \text{ M}^{-1}\text{cm}^{-1}$), complex **4**: 428 nm ($\epsilon = 2.0 \times 10^4 \text{ M}^{-1}\text{cm}^{-1}$). Likewise, each complex **5-7** (Figures **8-10**) exhibits an electronic absorption maxima between 449 – 459 nm when dissolved in DMSO (complex **5**: 459 nm ($\epsilon = 3.3 \times 10^4 \text{ M}^{-1}\text{cm}^{-1}$), complex **6**: 453 nm ($\epsilon = 2.5 \times 10^4 \text{ M}^{-1}\text{cm}^{-1}$), complex **7**: 449nm ($\epsilon = 1.1 \times 10^4 \text{ M}^{-1}\text{cm}^{-1}$)).

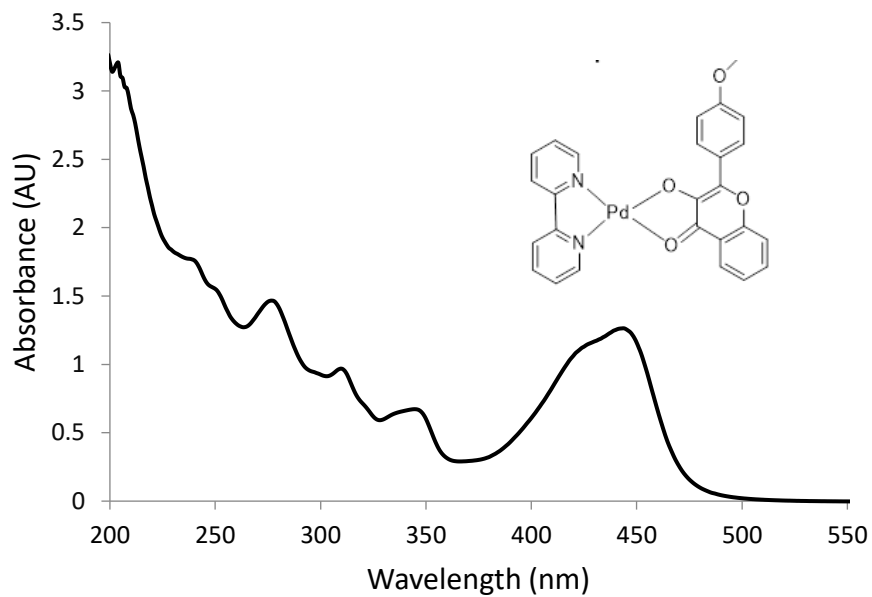


Figure 8. UV-Vis spectrum of complex 1 (50 μM in acetonitrile)

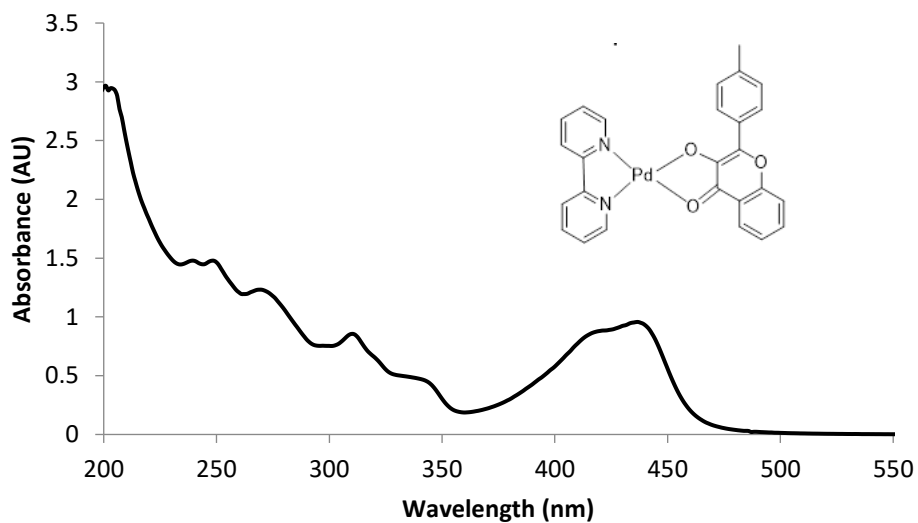


Figure 9. UV-Vis spectrum of complex 2 (50 μM in acetonitrile).

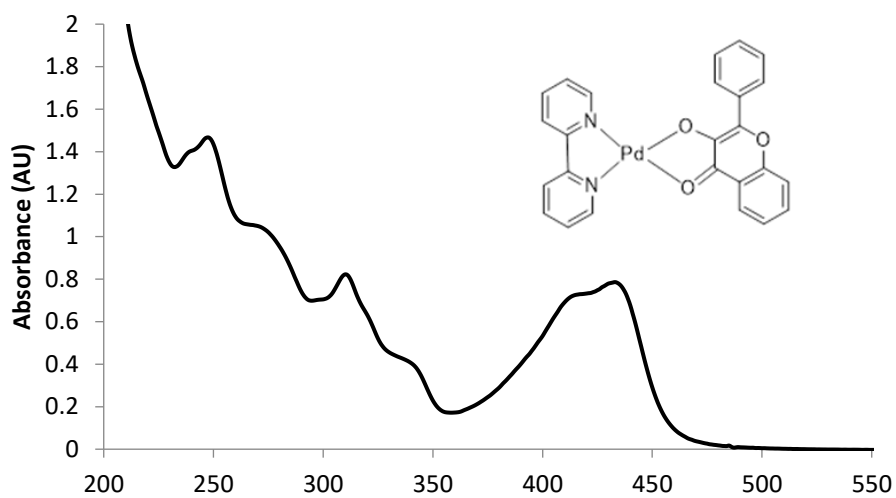


Figure 10. UV-Vis spectrum of complex **3** (50 μM in acetonitrile)

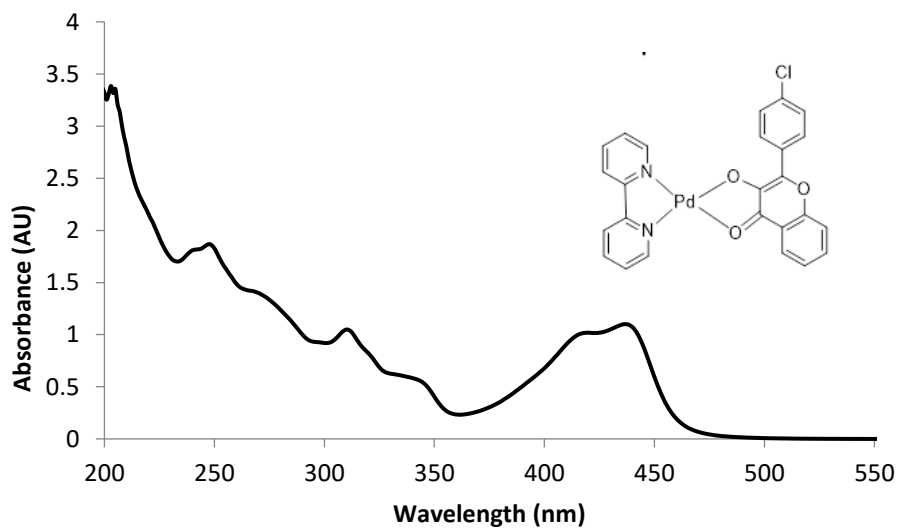


Figure 11. UV-Vis spectrum of complex **4** (50 μM in acetonitrile).

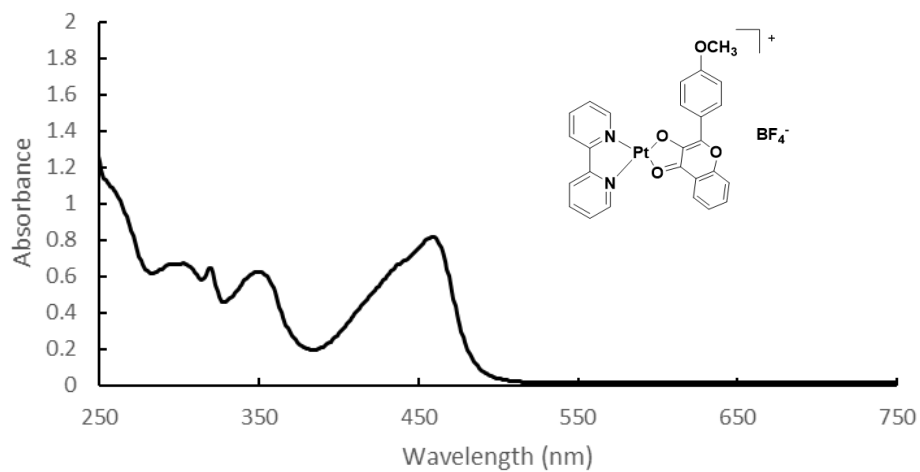


Figure 12. UV-Vis spectrum of complex **5** (25 μM in DMSO).

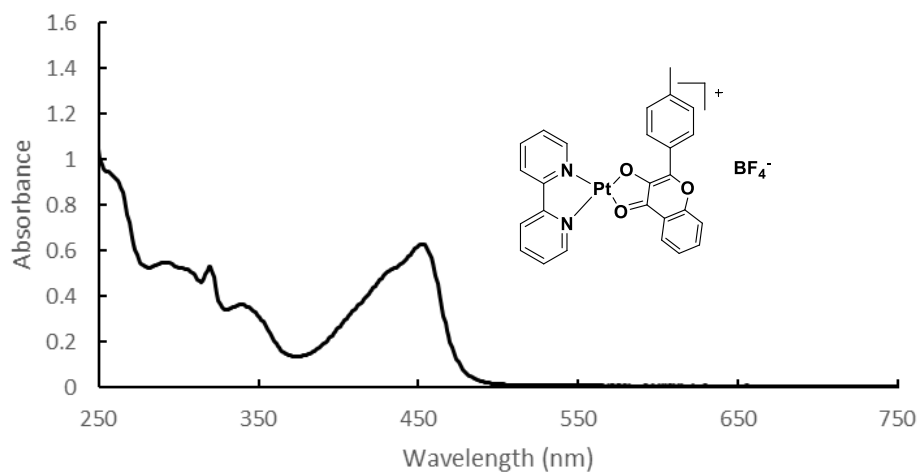


Figure 13. UV-Vis spectrum of complex **6** (25 μM in DMSO).

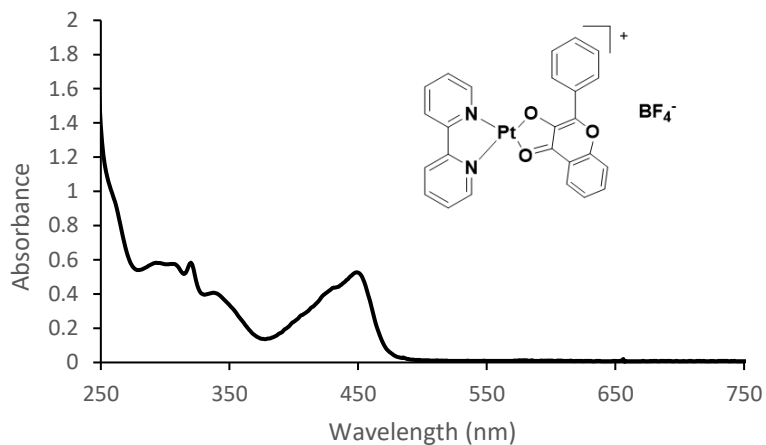


Figure 14. UV-Vis spectrum of complex **7** (25 μ M in DMSO).

The λ_{\max} of Pd(II) bipyridine flavonolate complexes $[\text{Pd}^{\text{II}}\text{BpyFla}^{\text{R}}]\text{BF}_4$ are red-shifted by 6–18 nm as compared to similar $[\text{Cu}^{\text{II}}\text{BpyFla}]\text{ClO}_4$, which was found to exhibit a square pyramidal geometry.⁵² This red-shift in the absorption band relative to neutral flavonol compounds can be explained by increased conjugation in the metal-ligand complex.¹⁷ The bands are blue-shifted about 30 nm relative to those of free flavonolate (458 nm for $\text{Me}_4\text{Nfla}^{18}$ and 465 nm for $\text{Kfla}^{53,54}$). Furthermore, the λ_{\max} values of the complexes are in order of $[\text{Pt}^{\text{II}}\text{BpyFla}^{\text{OMe}}]^+$ (**5**) > $[\text{Pt}^{\text{II}}\text{BpyFla}^{\text{Me}}]^+$ (**6**) > $[\text{Pt}^{\text{II}}\text{BpyFla}^{\text{H}}]^+$ (**7**) > $[\text{Pd}^{\text{II}}\text{BpyFla}^{\text{OMe}}]^+$ (**1**) > $[\text{Pd}^{\text{II}}\text{BpyFla}^{\text{Me}}]^+$ (**2**) > $[\text{Pd}^{\text{II}}\text{BpyFla}^{\text{H}}]^+$ (**3**) > $[\text{Pd}^{\text{II}}\text{BpyFla}^{\text{Cl}}]^+$ (**4**), and the plot of the λ_{\max} vs. Hammett constant σ for **1-4** is linear ($R = 0.98$) (Figure **15**). The plot of the λ_{\max} vs. Hammett constant σ for **5-7** is also linear ($R = 0.93$) (Figure **16**). The largest λ_{\max} was observed in complexes **1** and **5**, which have the strongest electron-donating group (OMe), presumably due to the best planarity and conjugation in flavonolate molecule, as confirmed by its smallest torsion angle in $[\text{Co}^{\text{II}}\text{L}^{\text{R}}\text{Fla}]$ complexes.³¹ These results indicate that the λ_{\max}

of the coordinated flavonolate is also affected by the electronic nature of the substituent group in the ligands.

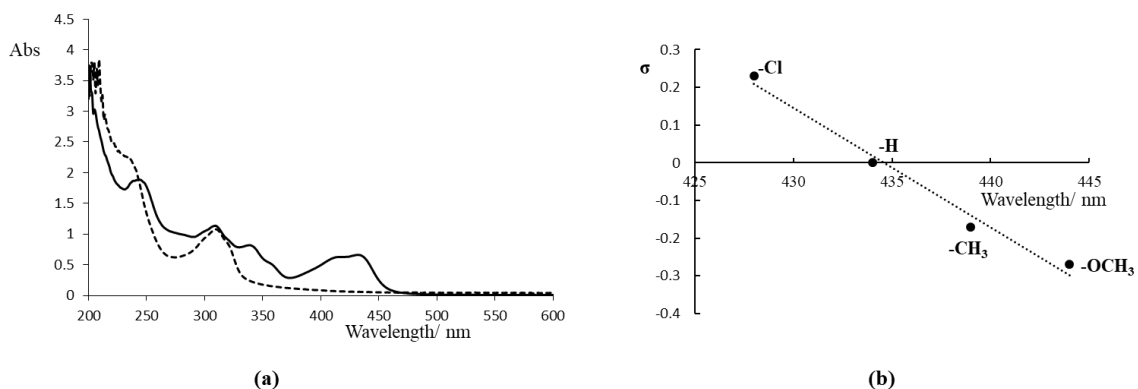


Figure 15. (a) UV-Vis spectrum of complex **3** (50 μM in acetonitrile, solid line) and product after reacting with O_2 in acetonitrile at 80°C (dashed line). (b) Plot of λ_{max} of the complexes vs. Hammett constant σ for complexes **1-4**.

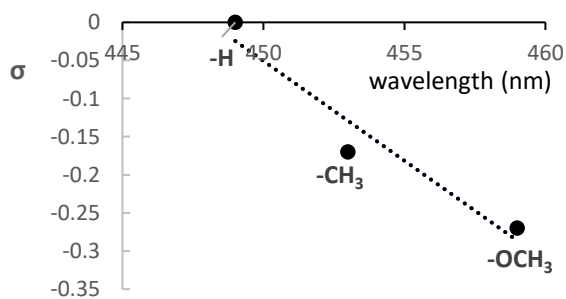


Figure 16. Plot of λ_{max} of the complexes vs. Hammett constant σ for complexes **5-7**.

Fluorescence spectroscopy of complexes **5-7** are shown in Figures **17-19**. The maximum excitation wavelength is 349.2 nm (**5**), 341.3 nm (**6**), and 340.8 nm (**7**). The maximum emission wavelength is 533.0 nm (**5**), 530.1 nm (**6**), and 527.4 nm (**7**). The Stokes shift is 183.8 nm (**5**), 188.8 nm (**6**), and 186.6 nm (**7**).

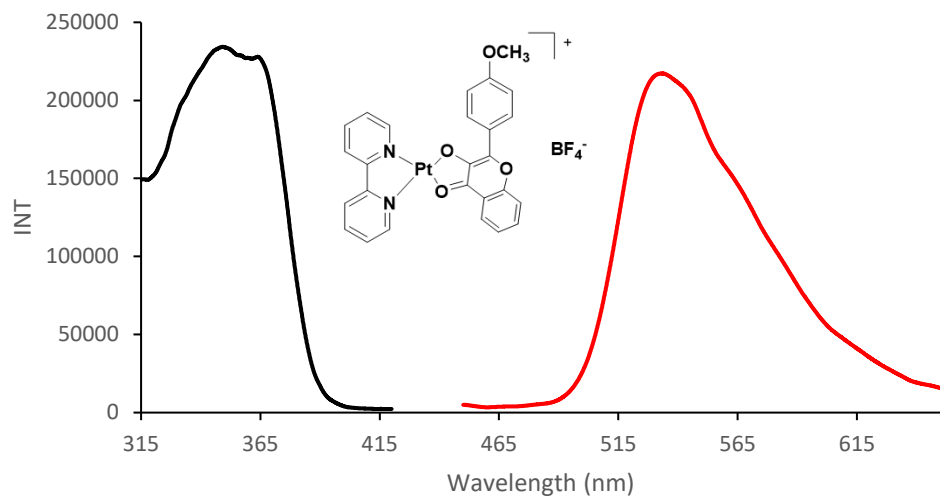


Figure 17. Fluorescence spectrum of complex 5.

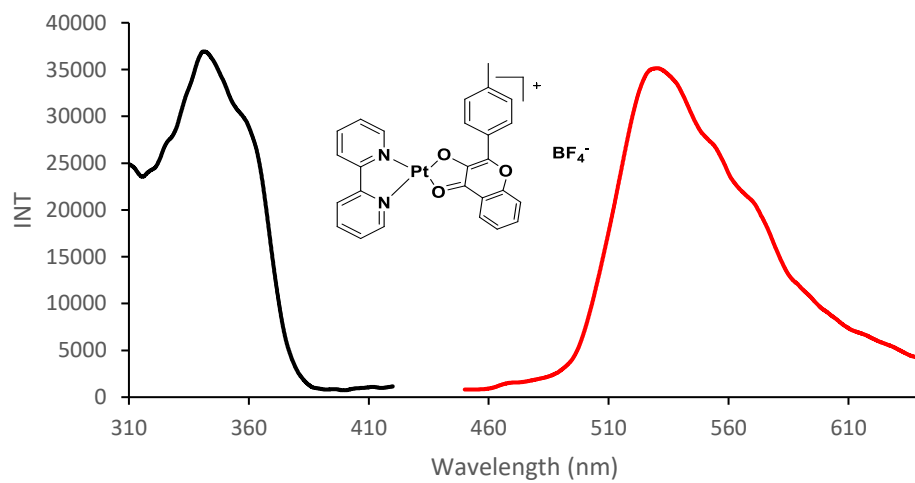


Figure 18. Fluorescence spectrum of complex 6.

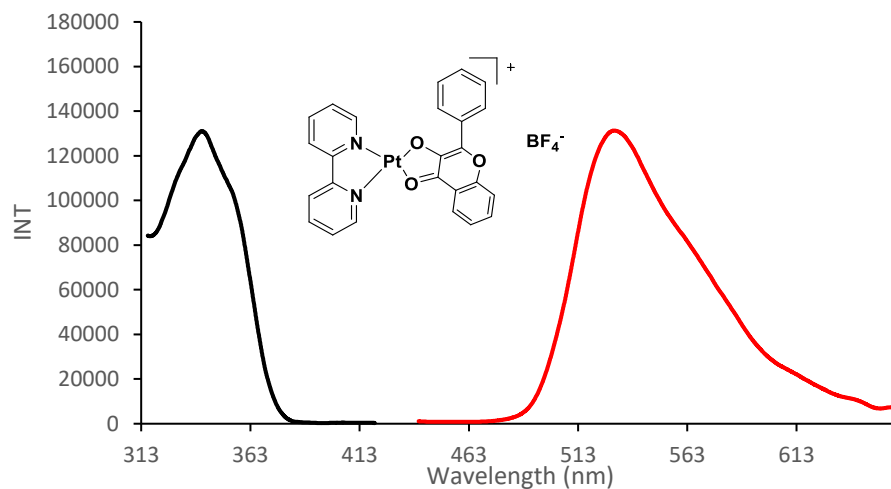


Figure 19. Fluorescence spectrum of complex **7**.

3.3 ESI-MS Spectrometry

The solution structures of the metal bipyridine flavonolate complexes were also examined by ESI-MS. Each complex shows one peak cluster that can be assigned to $[\text{Pd}^{\text{II}}\text{BpyFla}^{\text{R}}]^+$ (m/z (pos.) = 529.04 for **1**, 513.04 for **2**, 499.03 for **3**, and 532.99 for **4**) and to $[\text{Pt}^{\text{II}}\text{BpyFla}^{\text{R}}]^+$ (m/z (pos.) = 618.10 for **5**, 602.10 for **6**, and 588.09 for **7**). The m/z value and isotope distribution pattern of each peak cluster match well with the calculated value (Figures **20-26**), indicating that each complex keeps its oxidation state and mononuclear structure in solution.

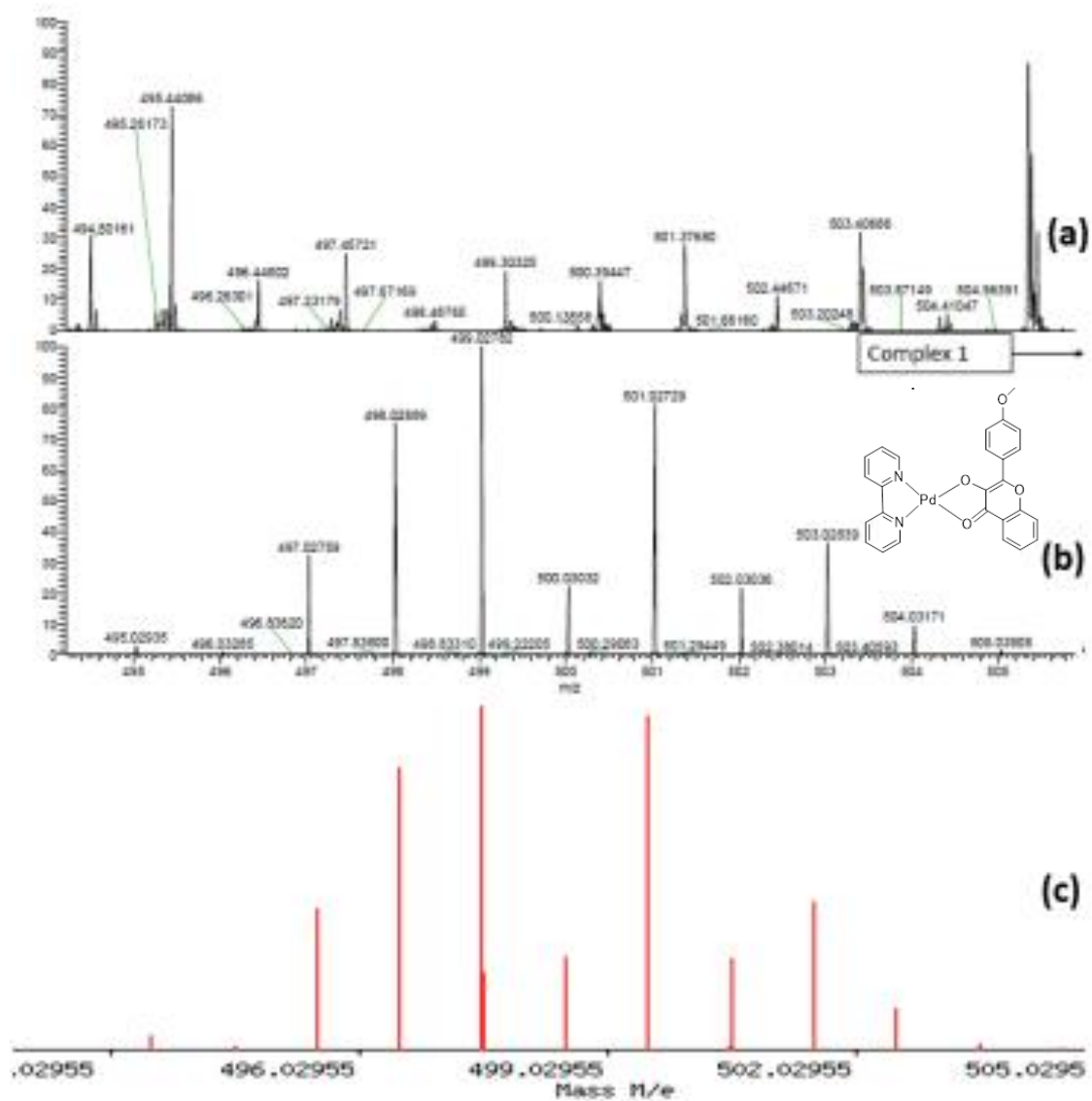


Figure 20. (a) Zoomed blank mass spectrum before sample. (b) Zoomed isotope pattern on mass spectrum of complex **1**. (c) Zoomed theoretical isotope distribution of complex **1**.

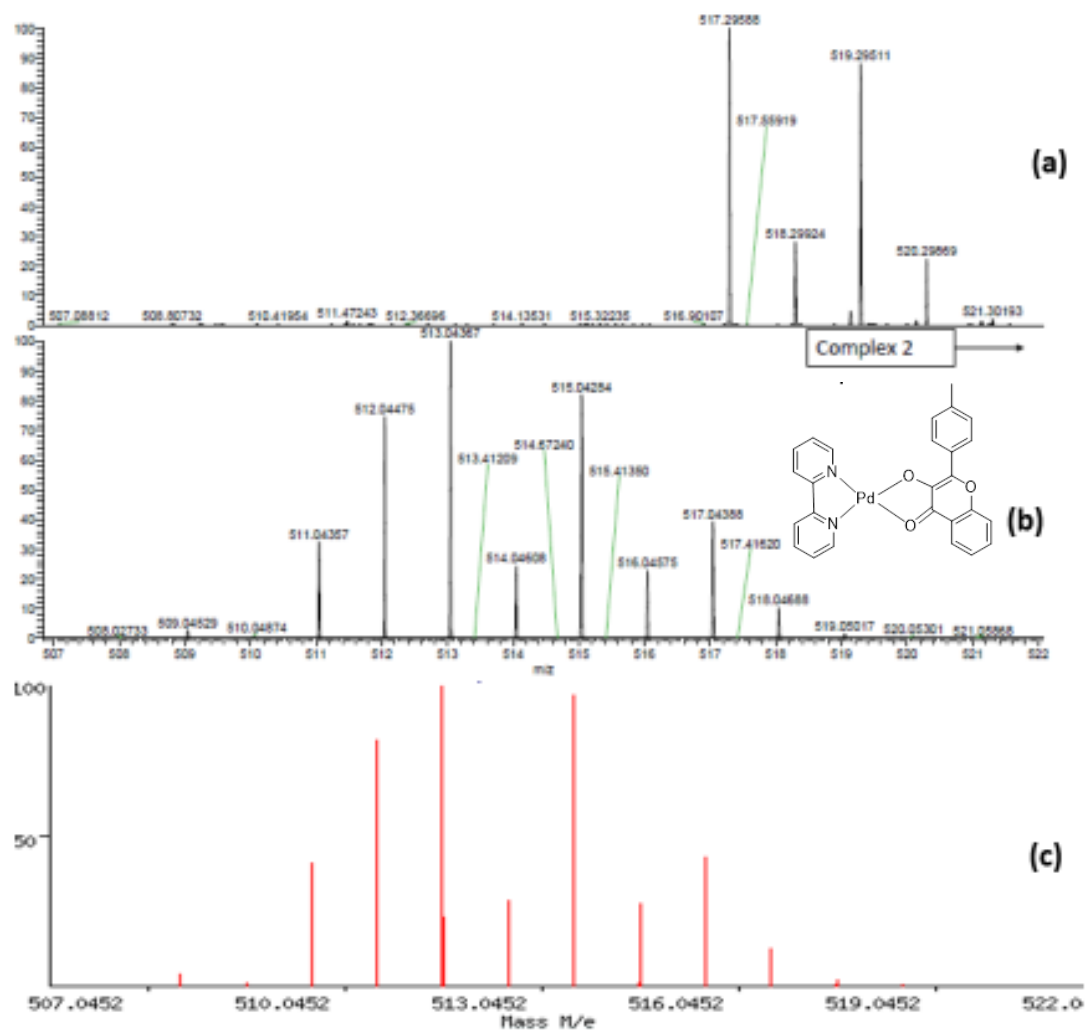


Figure 21. (a) Zoomed blank mass spectrum before sample. (b) Zoomed isotope pattern on mass spectrum of complex 2. (c) Zoomed theoretical isotope distribution of complex 2.

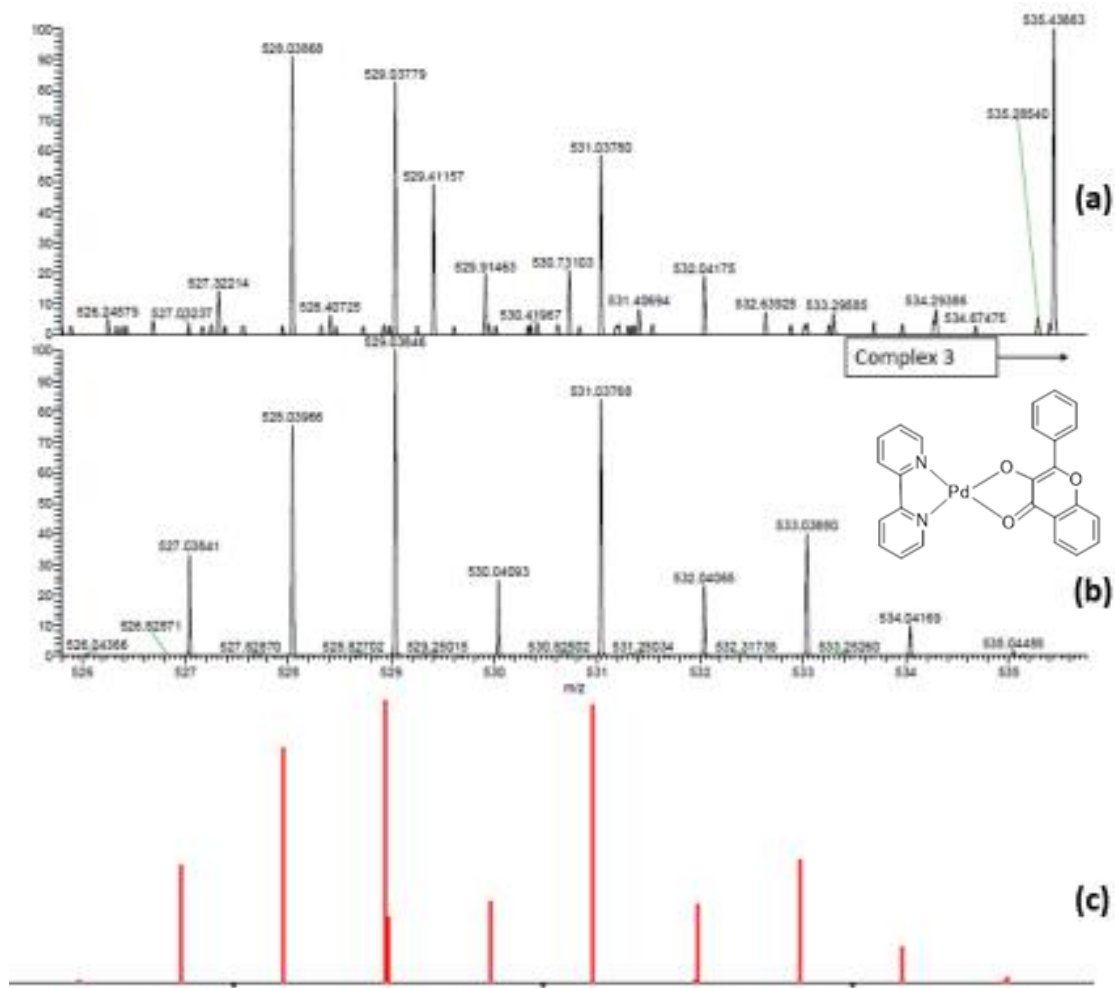


Figure 22. (a) Zoomed blank mass spectrum before sample. (b) Zoomed isotope pattern on mass spectrum of complex 3. (c) Zoomed theoretical isotope distribution of complex 3.

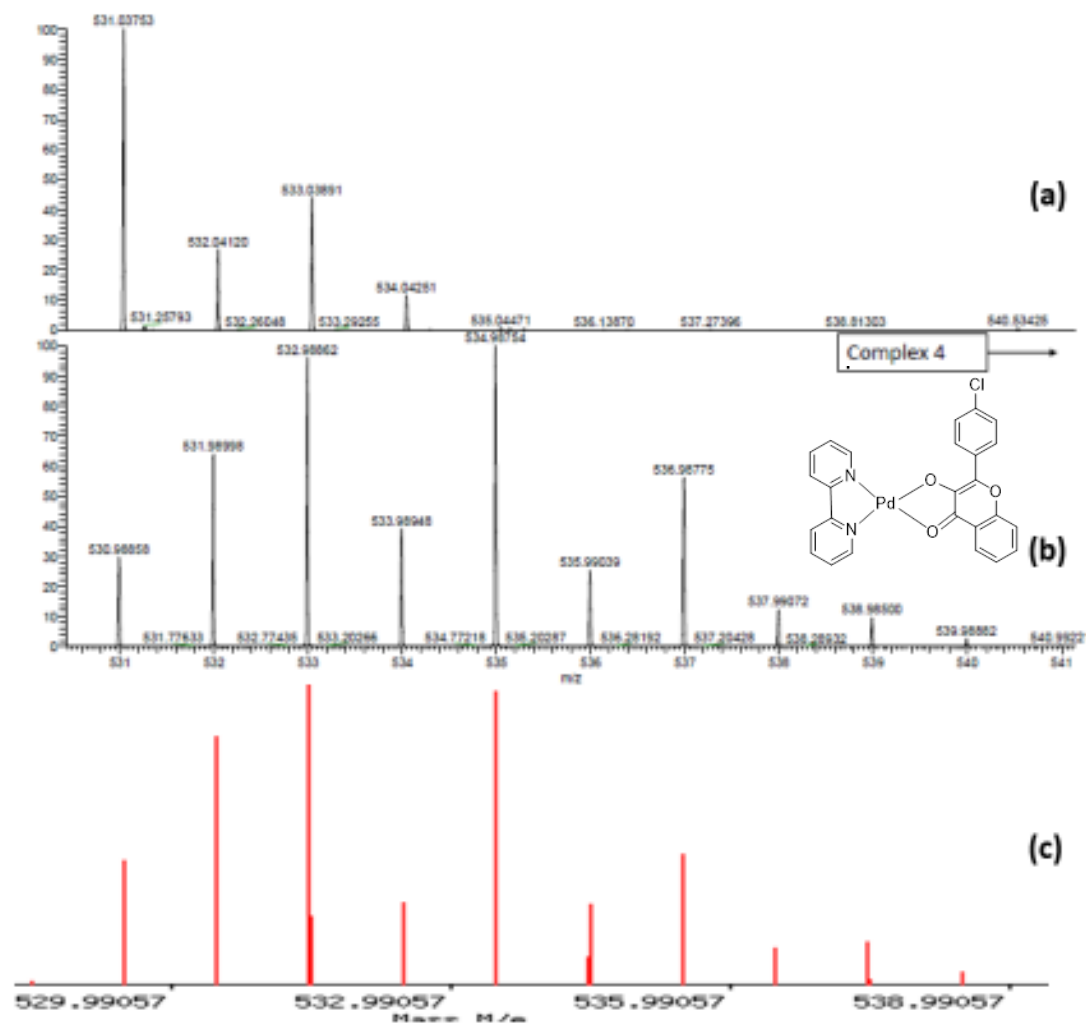


Figure 23. (a) Zoomed blank mass spectrum before sample. (b) Zoomed isotope pattern on mass spectrum of complex **4**. (c) Zoomed theoretical isotope distribution of complex **4**.

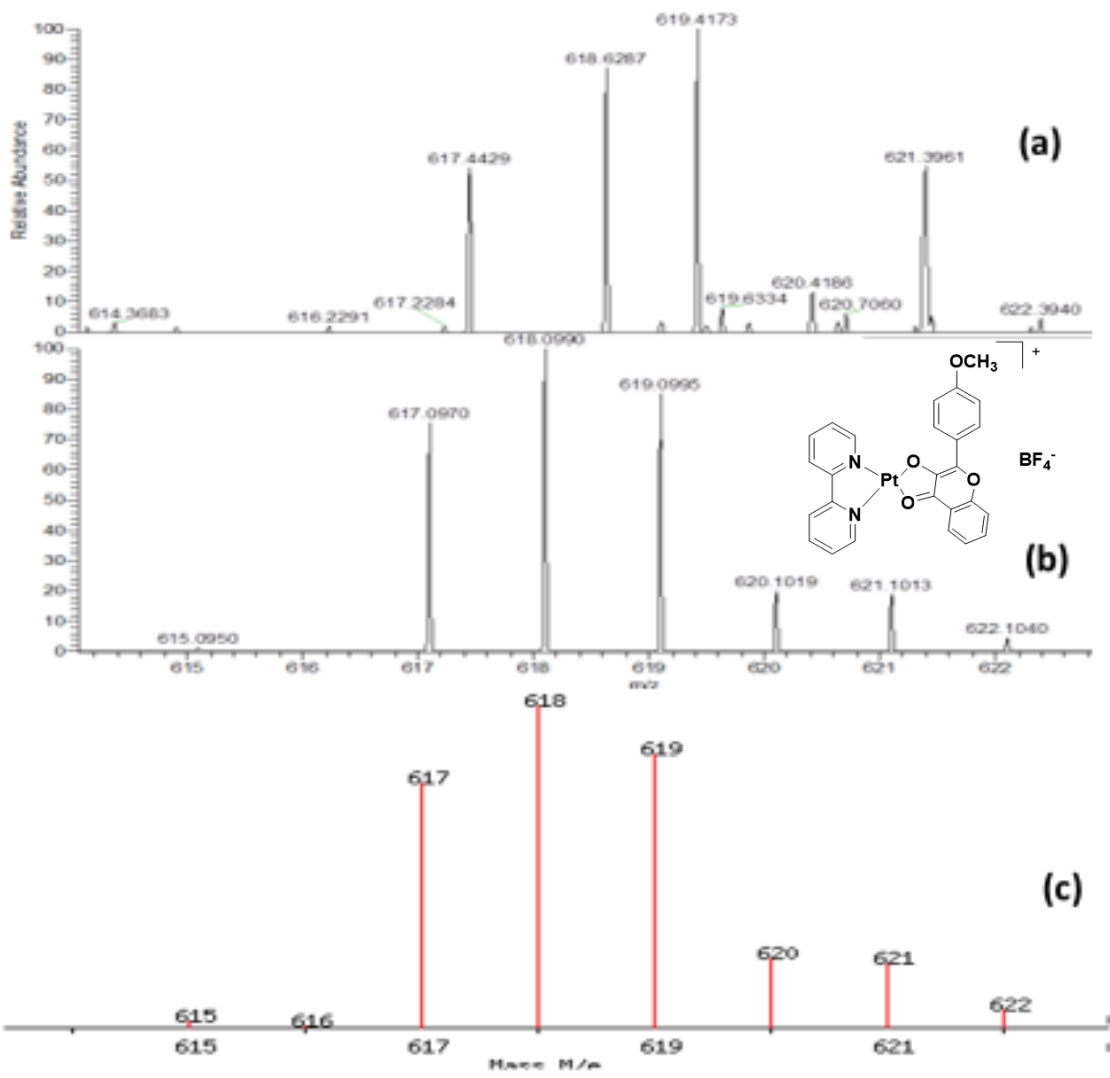


Figure 24. (a) Zoomed blank mass spectrum before sample. (b) Zoomed isotope pattern on mass spectrum of complex **5**. (c) Zoomed theoretical isotope distribution of complex **5**.

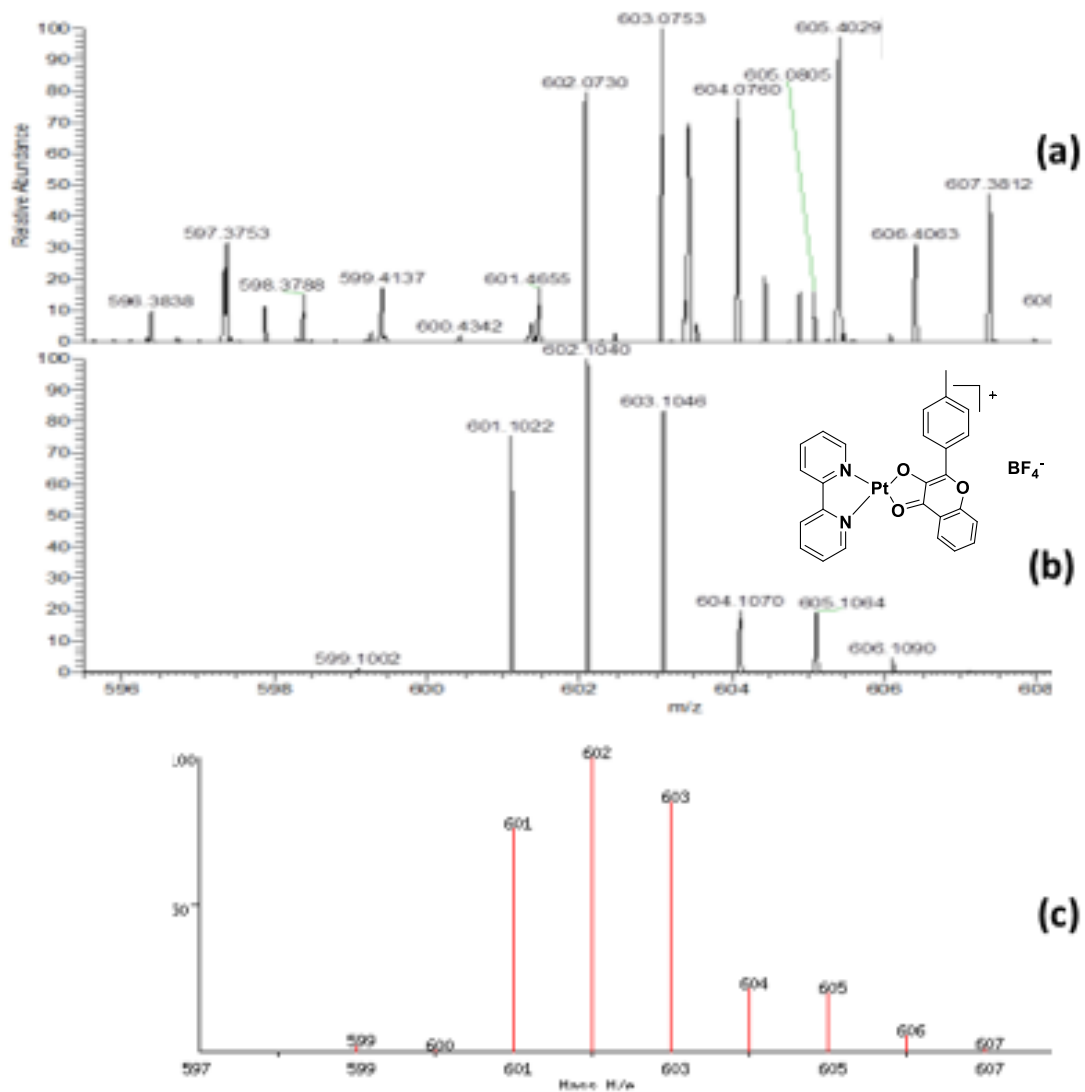


Figure 25. (a) Zoomed blank mass spectrum before sample. (b) Zoomed isotope pattern on mass spectrum of complex 6. (c) Zoomed theoretical isotope distribution of complex 6.

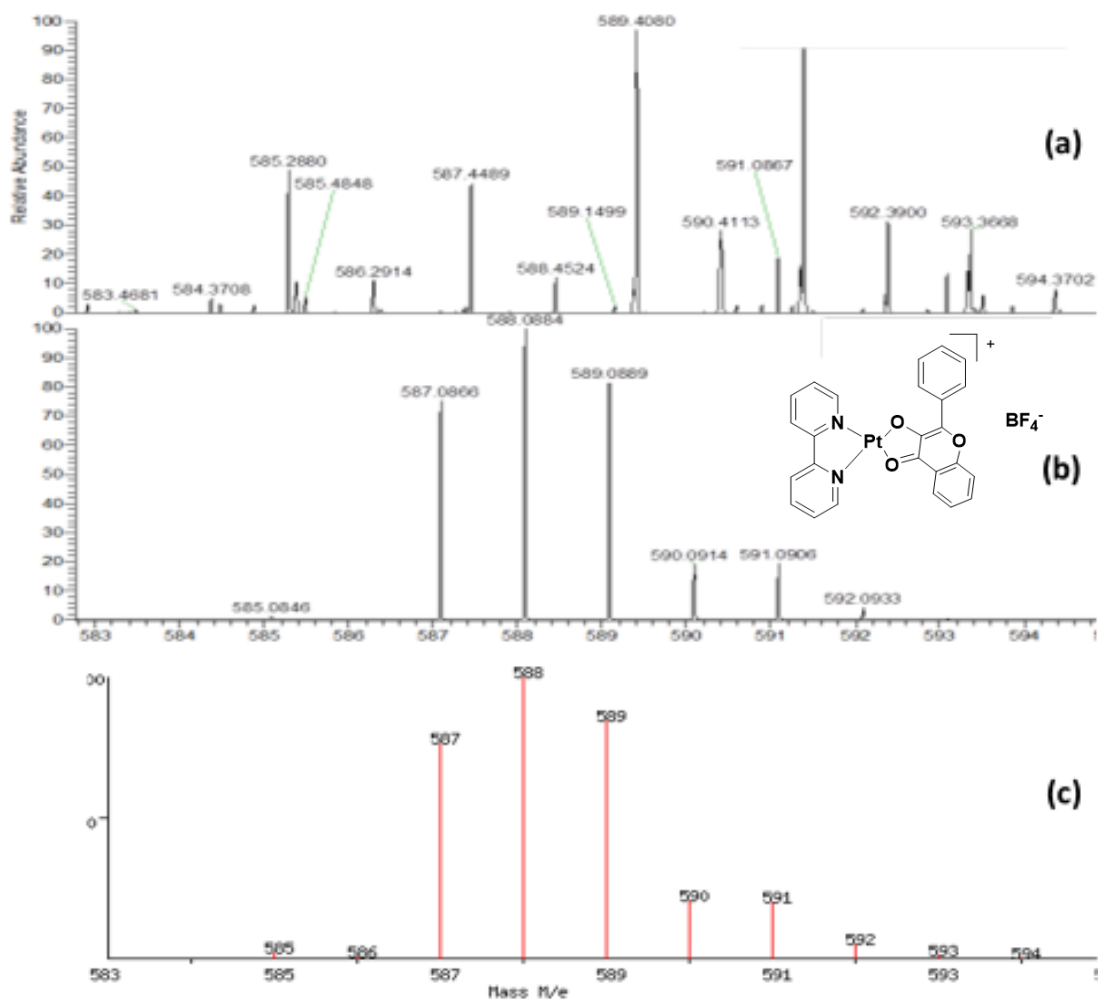


Figure 26. (a) Zoomed blank mass spectrum before sample. (b) Zoomed isotope pattern on mass spectrum of complex **7**. (c) Zoomed theoretical isotope distribution of complex **7**.

3.4 NMR spectroscopy

More conclusive structural information was obtained from NMR analysis of the complexes (Figures **27-38**). $^1\text{H-NMR}$ and $^{13}\text{C-NMR}$ spectra of complex **3** are shown in Figure **27** and Figure **28**, respectively. In the $^1\text{H-NMR}$ spectrum, 17 protons are seen in

complex **3**. Assignment of each proton peak was confirmed by ^1H - ^1H COSY and ^1H - ^{13}C HSQC (Figures **29-30**). Complex **7** has a very similar ^1H -NMR spectrum, shown in Figure **37**. The ^1H -NMR spectra of complexes **1,2,4-6** (Figures **32-36**) are similar but with a signal upfield for the more shielded protons on the methyl and methoxy substituents of the flavonolate.

In the ^{13}C -NMR spectrum of complex **3** (Figure **28**), there are 8 quaternary C atoms: 2 (C20 and C21) from bipyridyl and 6 (C1, C2, C7, C8, C9, and C10) from the flavonolate. In addition, there are 17 tertiary C atoms, all of which were assigned by ^1H - ^{13}C HSQC. The assignment of all C atoms and H atoms were doubly confirmed by C-H long-range couplings obtained from the ^1H - ^{13}C HMBC spectrum (Figure **31**). The analogous ^{13}C -NMR spectrum of complex **7** (Figure **38**) is very similar.

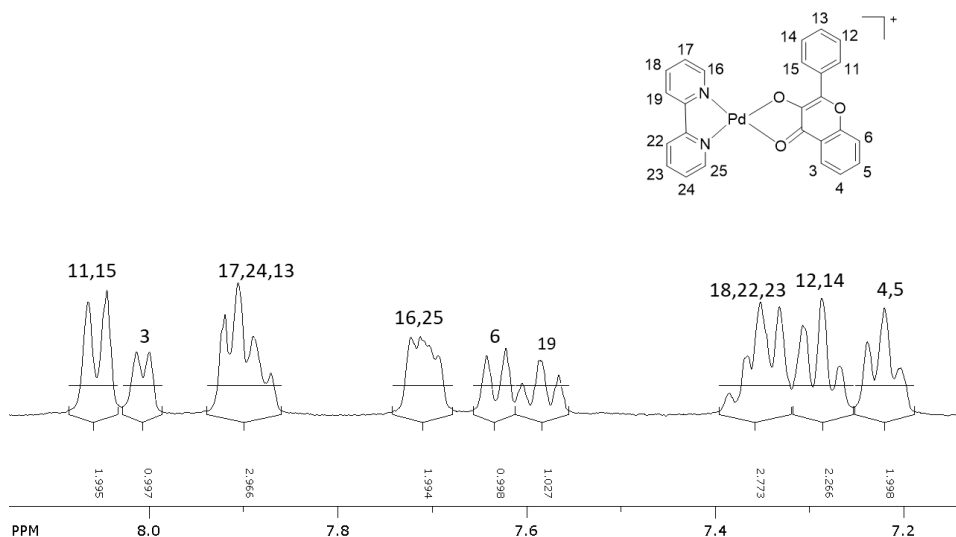


Figure 27. ^1H NMR spectrum of complex **3**.

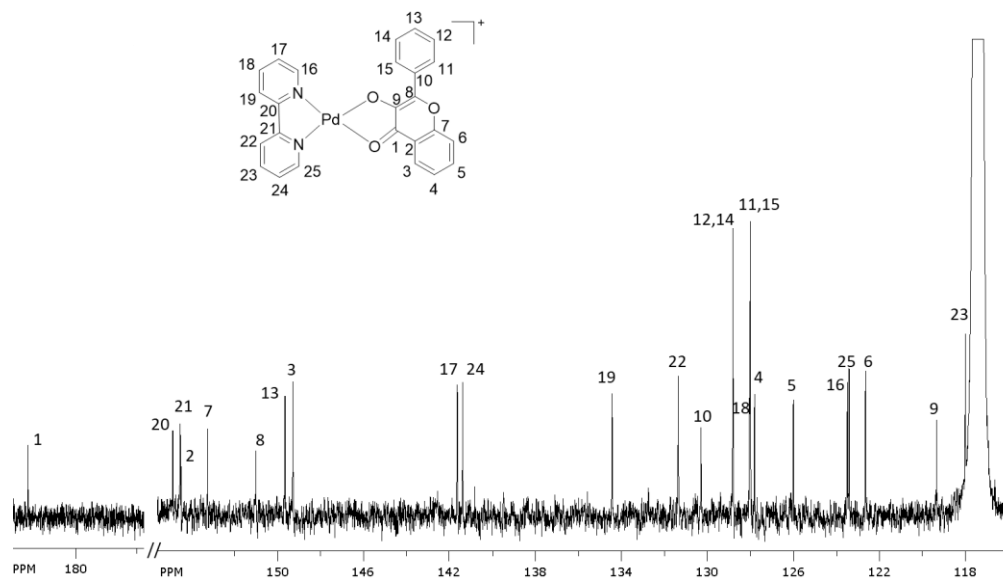


Figure 28. ^{13}C NMR spectrum of complex 3.

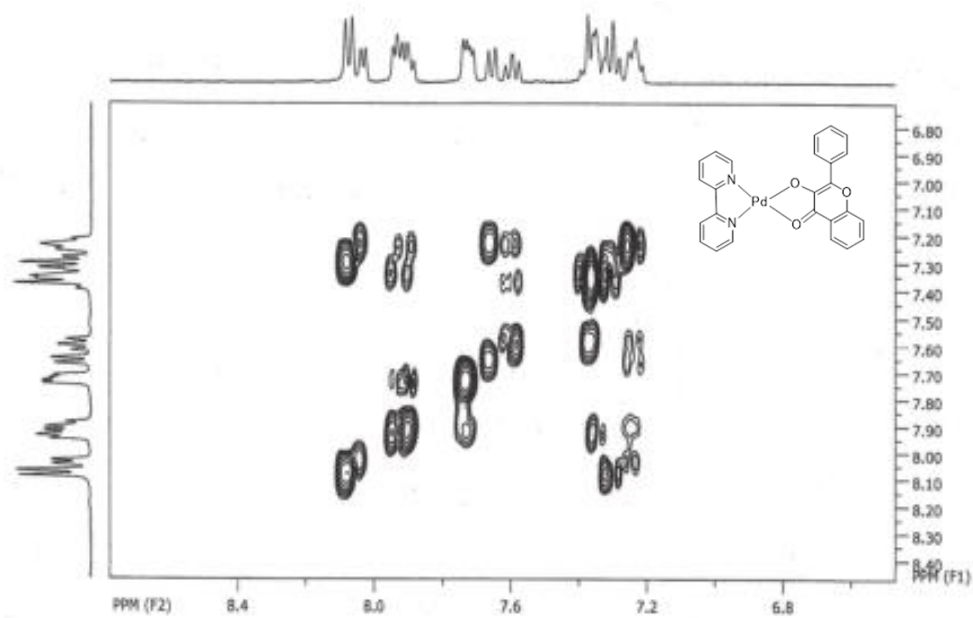


Figure 29. 2D ^1H - ^1H COSY of complex 3.

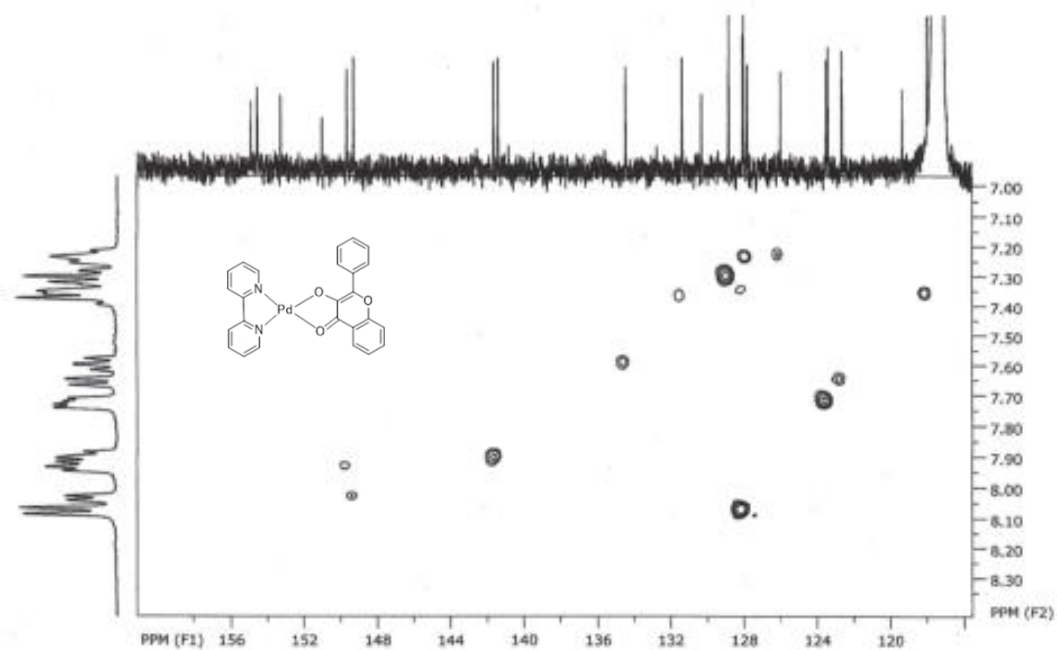


Figure 30. 2D ^{13}C - ^1H HSQC of complex 3.

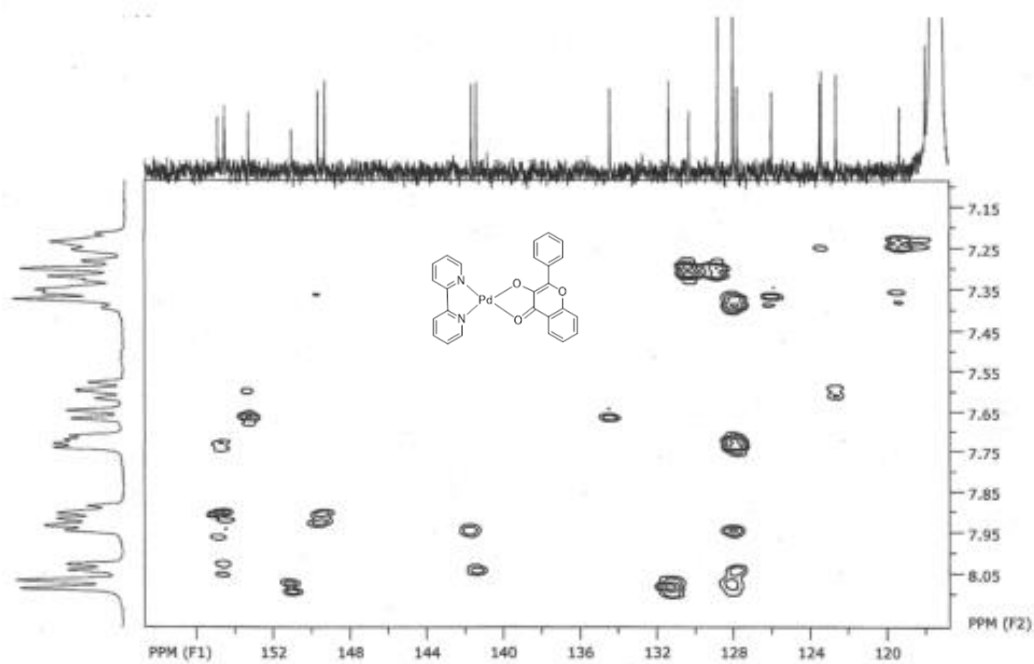


Figure 31. 2D ^{13}C - ^1H HMBC of complex 3.

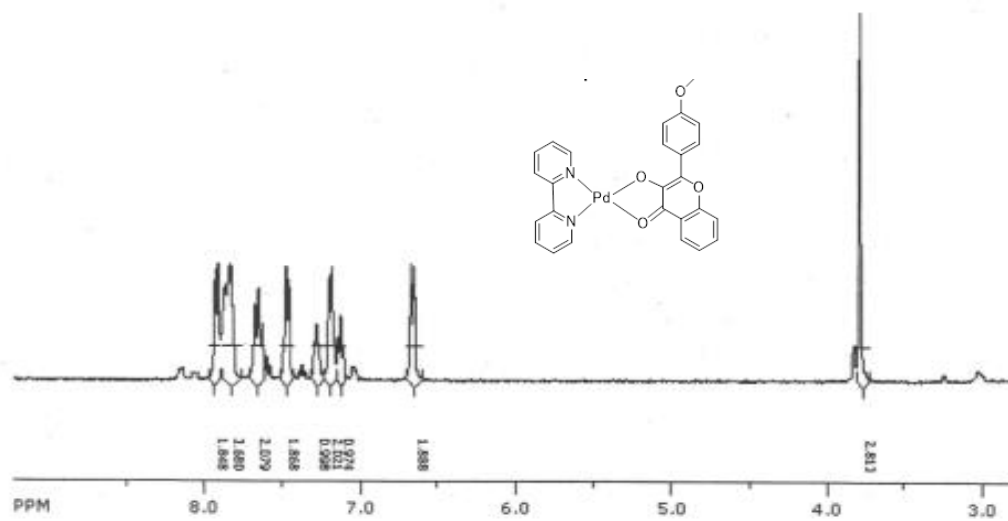


Figure 32. ^1H NMR spectrum of complex 1.

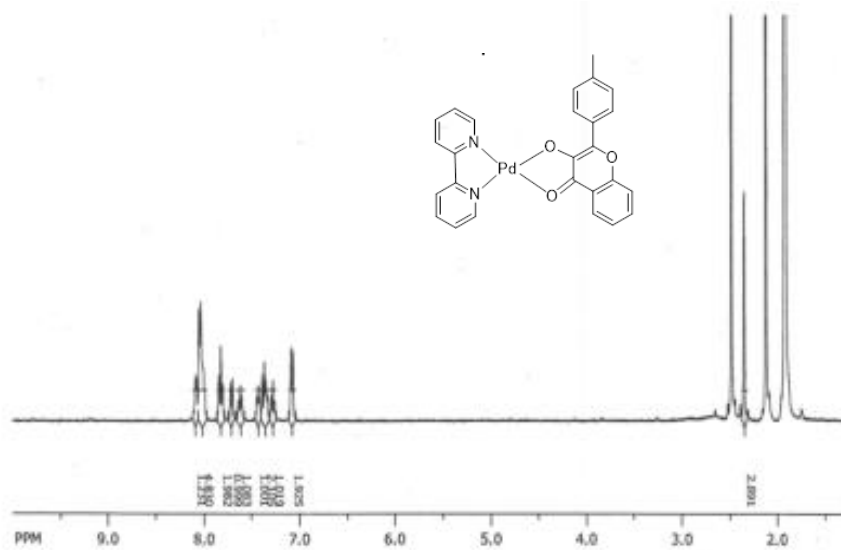


Figure 33. ^1H NMR spectrum of complex 2.

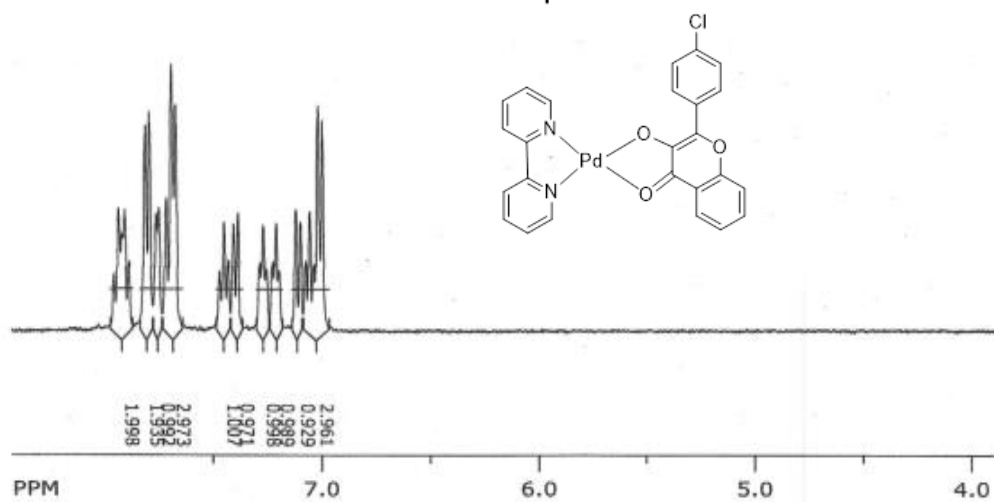


Figure 34. ^1H NMR spectrum of complex **4**.

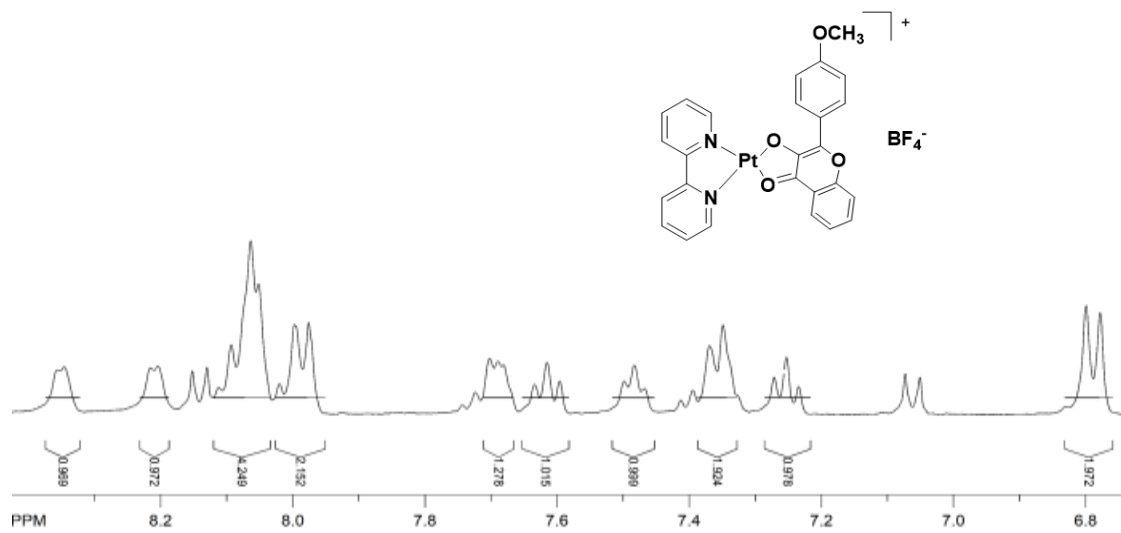


Figure 35. ^1H NMR spectrum of complex **5** in CD_3CN .

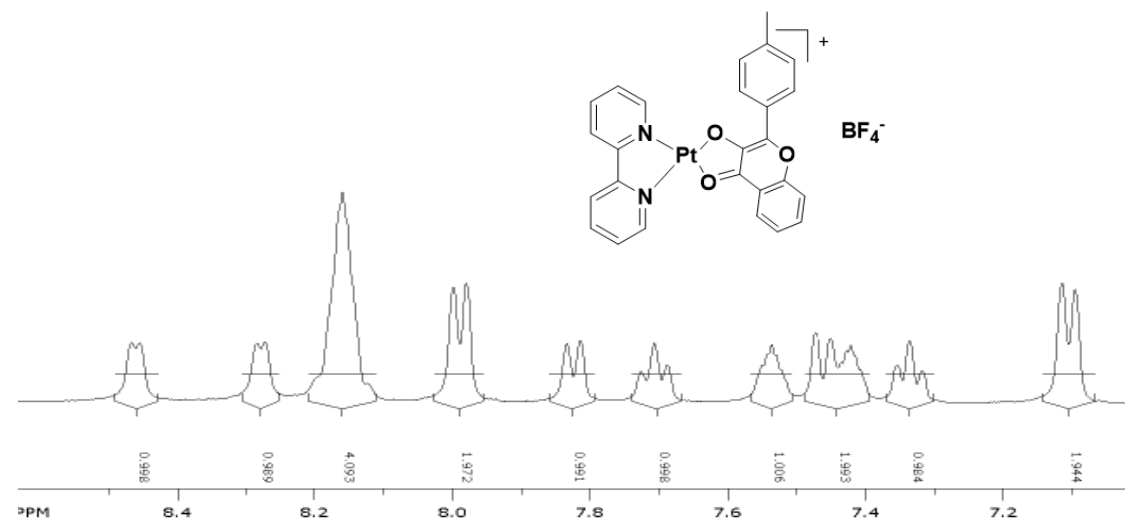


Figure 36. ^1H NMR spectrum of complex **6** in CD_3CN .

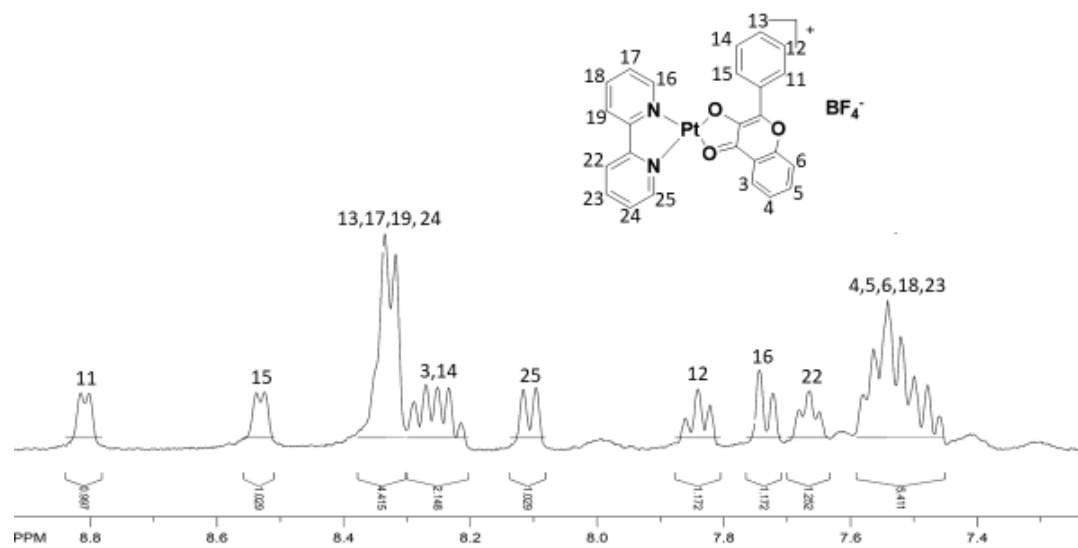


Figure 37. ^1H NMR spectrum of complex **7** in CD_3CN .

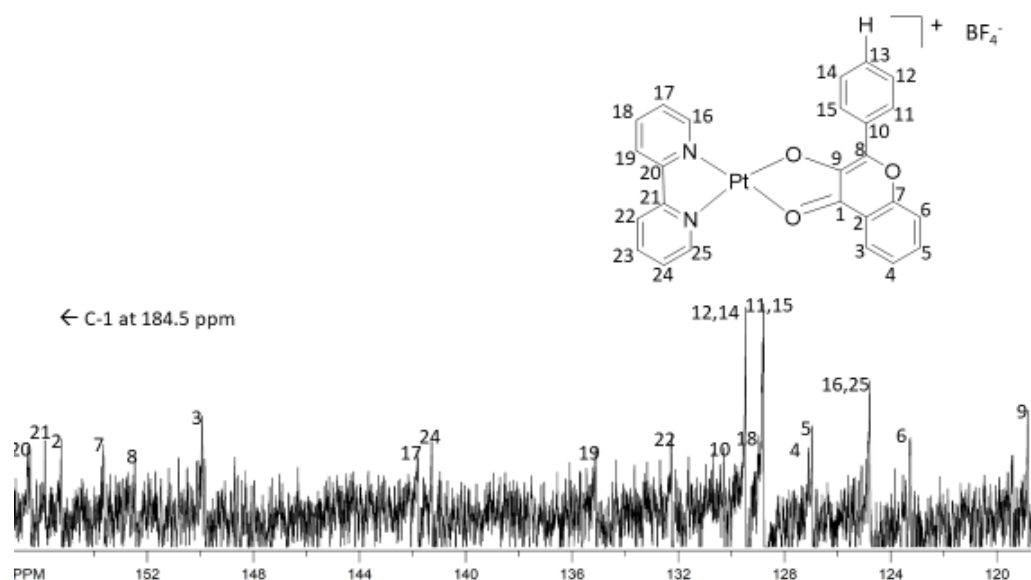


Figure 38. ^{13}C NMR spectrum of complex **7** in $(\text{CD}_3)_2\text{SO}$.

3.5 Oxygenation of Pd(II) bipyridine flavonolate complexes with O_2

The oxygenation reaction of Pd(II) bipyridine flavonolate complexes was followed by monitoring the decrease of the absorbance of the coordinated flavonolate ($\pi - \pi^*$) at the corresponding λ_{max} . At room temperature, no oxygenation reaction between Pd(II) bipyridine flavonolate complexes and dioxygen occurred, as seen in Figures **39-42**. However, if the reaction is carried out at elevated temperature ($80\text{ }^\circ\text{C}$), the decay of coordinated flavonolate band was observed (Figure **15a**). The similar reactivity was observed in the reaction of $[\text{Cu}^{\text{II}}\text{BpyFla}]\text{ClO}_4$ with dioxygen in acetonitrile, indicating a big energy barrier to overcome for metal bipyridine flavonolate complexes and ground state dioxygen ($^3\text{O}_2$)⁵². A UV-Vis lamp with broad band light (300 nm–900 nm) was used to examine the effect of light on the reaction between $[\text{Pd}^{\text{II}}\text{BpyFla}]\text{BF}_4$ and dioxygen.

However, unlike the reaction of $[\text{Ru}^{\text{II}}(\text{Bpy})_2\text{Fla}]\text{PF}_6$ with dioxygen in which light speeds up the reaction rate³³, the oxygenation reaction of $[\text{Pd}^{\text{II}}\text{BpyFla}^{\text{R}}]\text{BF}_4$ was still very slow under light. There is no difference between oxygenation reaction of Pd(II) bipyridine flavonolate complexes with or without light, implying that light has no effect on reaction of $[\text{PdBpyFla}]\text{BF}_4$ with dioxygen.

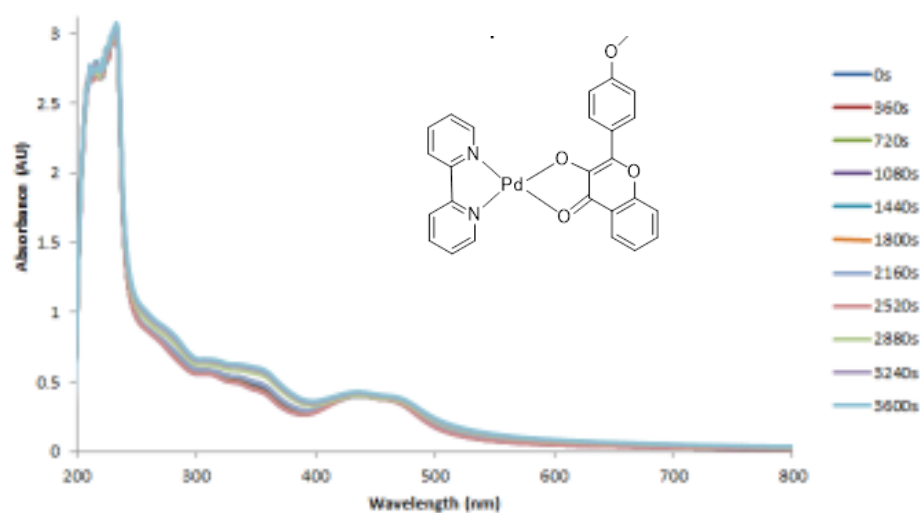


Figure 39. UV-Vis absorption spectra of reaction between complex **1** and O₂ with light irradiation under Ar in acetonitrile.

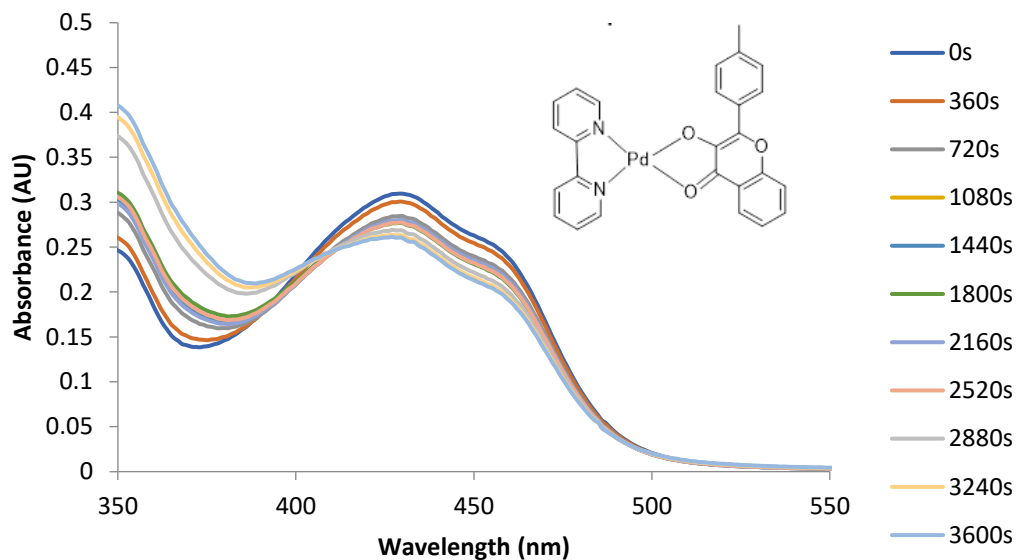


Figure 40. UV-Vis absorption spectra of reaction between complex **2** and O₂ with light irradiation under Ar in acetonitrile.

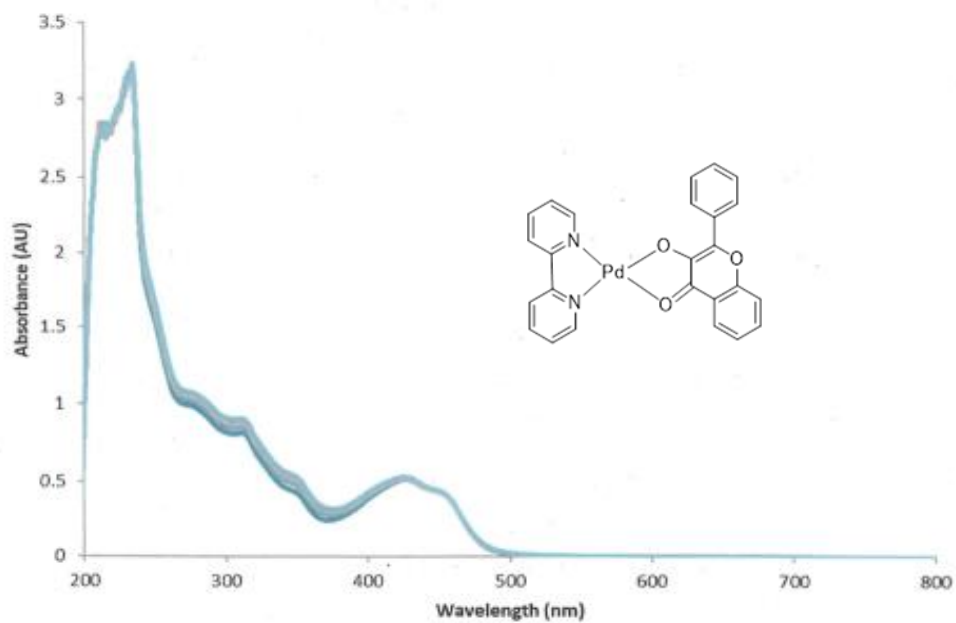


Figure 41. UV-Vis absorption spectra of reaction between complex **3** and O₂ with light irradiation under Ar in acetonitrile.

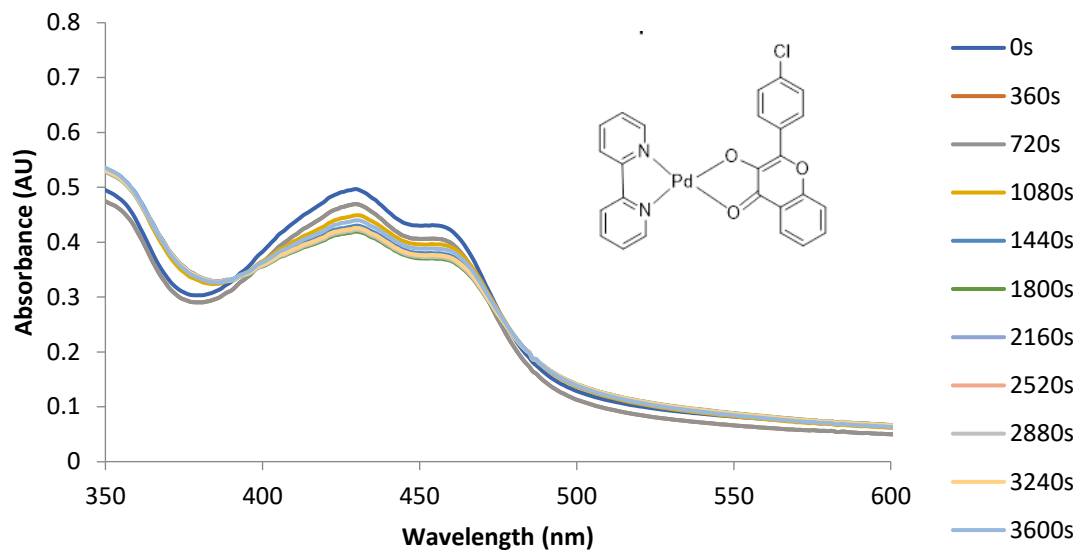


Figure 42. UV-Vis absorption spectra of reaction between complex **4** and O₂ with light irradiation under Ar in acetonitrile.

3.6 Oxygenation of Pt(II) bipyridine flavonolate complexes with O₂

The oxygenation reaction of Pt(II) bipyridine flavonolate complexes was investigated. Changes in the electronic absorbance at λ_{max} as a function of irradiation time were monitored. There was no oxygenation reaction without irradiation. A decrease in the intensity of the MLCT peak (e.g. 459 nm for complex **5**) as the complexes were exposed to broadband (300 nm–900 nm) excitation using the Rayonet photoreactor at room temperature indicates all three complexes reacted with dioxygen (Figures **43-45**).

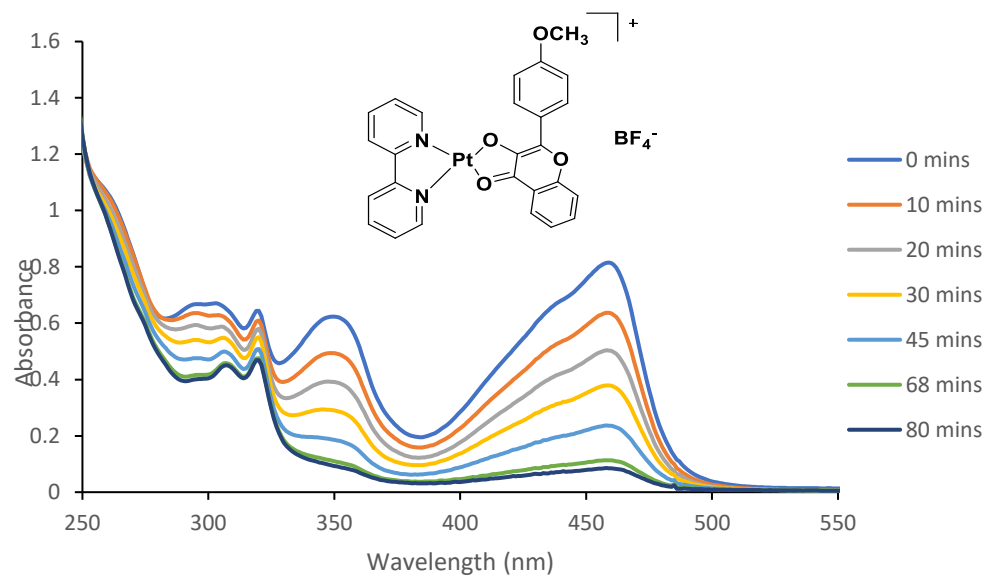


Figure 43. UV-Vis absorption spectra of reaction between complex **5** (25 μM) in DMSO and O₂ with light irradiation at ambient temperature.

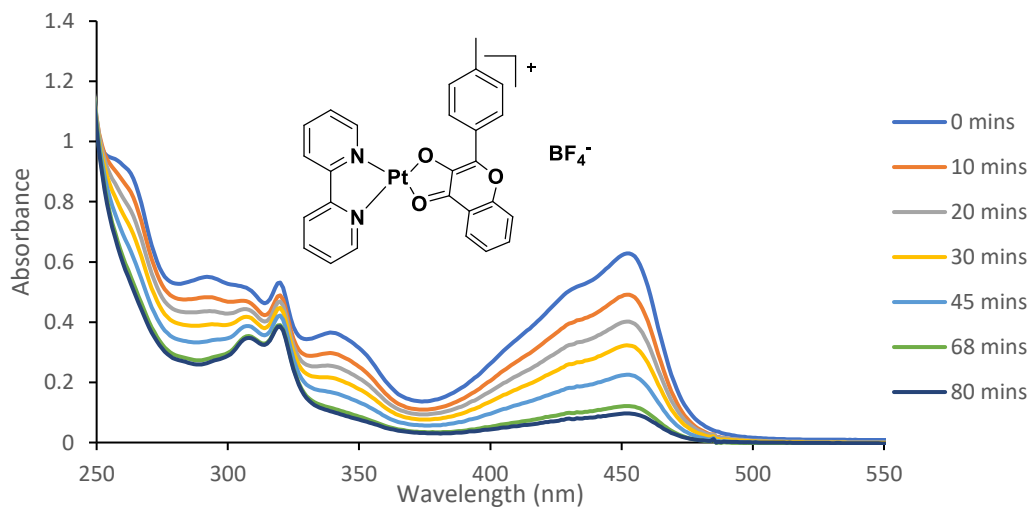


Figure 44. UV-Vis absorption spectra of reaction between complex **6** (25 μM) in DMSO and O₂ with light irradiation at ambient temperature.

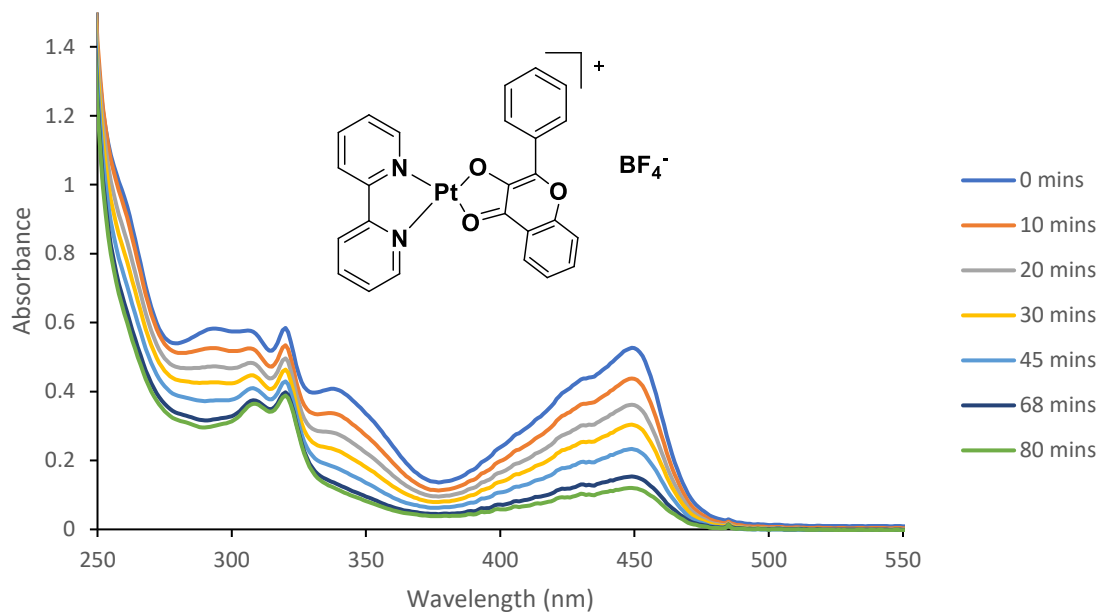


Figure 45. UV-Vis absorption spectra of reaction between complex **7** (25 μM) in DMSO and O₂ with light irradiation at ambient temperature.

The solutions turned from yellow-green to colorless, indicating light catalyzes the [Pt^{II}(Bpy)Fla]BF₄ oxygenation reaction. This is similar to a previously reported photo-induced reaction of [(L)Zn(3-Hfl)ClO₄] (L is a bidentate nitrogen donor ligand) reacting with oxygen.⁵⁵ Since the platinum complexes underwent oxygenation reaction with irradiation at room temperature but the palladium complexes did not, the platinum complexes absorb the required activation energy, but the palladium complexes do not. This is reasonable because energy is inversely related to wavelength. The platinum complexes have a higher λ_{max} than the palladium complexes, so the platinum complexes must be at a lower energy in their excited state compared to palladium in its excited state.

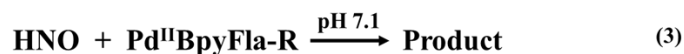
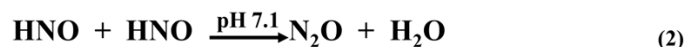
The energy barrier was also lower in complexes with electron-donating groups in the *para* position of the flavonolato moiety, reflected in the larger λ_{max} value of the methoxyflavonolate complexes **1** and **5**. These results indicate that the increased electron density on the flavonolato ligand by *para* electron-donating substituents raises the energy of the metal's HOMO and shifts the π - π^* absorption to lower energies, effectively lowering the energy barrier for electron transfer to O₂.^{55,56} The proposed mechanism of CO release involves platinum serving as a conduit for a single electron transfer from the flavonolate ligand to the dioxygen ligand, creating two radicals. The superoxide radical would attack the flavonolate radical to form a bridging peroxo species, similar to the mechanism of Cu^{II} fungal quercetin dioxygenases.⁵⁵ Following oxidative cleavage of this bridge, CO would be extruded and a depside formed.

3.7 Nitroxygenation of Pd(II) bipyridine flavonolate complexes with HNO

The simple molecule nitrosyl hydride (HNO) is the singly reduced and protonated form of nitric oxide, NO. HNO has been reported to have similar reactivity with dioxygen because it can be trapped by various O₂-binding globins and interact with O₂-dependent oxygenases.^{41,57} Previous publication shows that HNO can substitute dioxygen in the reaction with free flavonol. Nitroxygenation reaction of free flavonol (quercetin) with HNO is much faster than that with dioxygen.⁵⁸ The reaction of Pd(II) bipyridine flavonolate complexes with HNO was investigated to provide insights on reactivity of HNO.

Following the typical procedure in a nitroxygenation assay, solutions of complex **3** and Angeli's salt were mixed in deaerated pH 7 phosphate buffer. The decrease in

concentration of complex **3** was followed by the decrease in its absorbance at 434 nm. Figures **46-49** shows the reaction spectra of $[\text{Pd}^{\text{II}}\text{BpyFla}^{\text{R}}]\text{BF}_4$ with Angeli's salt (AS), HNO donor, in 50mM phosphate buffer. As opposed to oxygenation reaction of Pd(II) bipyridine flavonolate complexes with dioxygen at high temperature (80 °C), nitroxylation reaction of $[\text{Pd}^{\text{II}}\text{BpyFla}]\text{BF}_4$ occurred at room temperature with a fast rate. Initial kinetic analysis was performed and analyzed using the sequential reactions depicted in equations **1-3**. Rate analysis of nitroxylation reactivity is complicated by the slow decomposition rate of the HNO-donor Angeli's salt and the competitive dimerization of free HNO. The slow release of HNO from Angeli's salt would be predicted as the rate-limiting step, but at relatively low substrate concentrations, the initial rate of reaction is dependent on both $[\text{Pd}^{\text{II}}\text{BpyFla}]^+$ and [AS].



To ascertain that the CO release was due to the complex rather than another substance in solution, a control reaction was performed with the nitrite ion (Figure **50**). There was little decrease in absorbance at λ_{max} ; nitrite ions did not cause the release of CO.

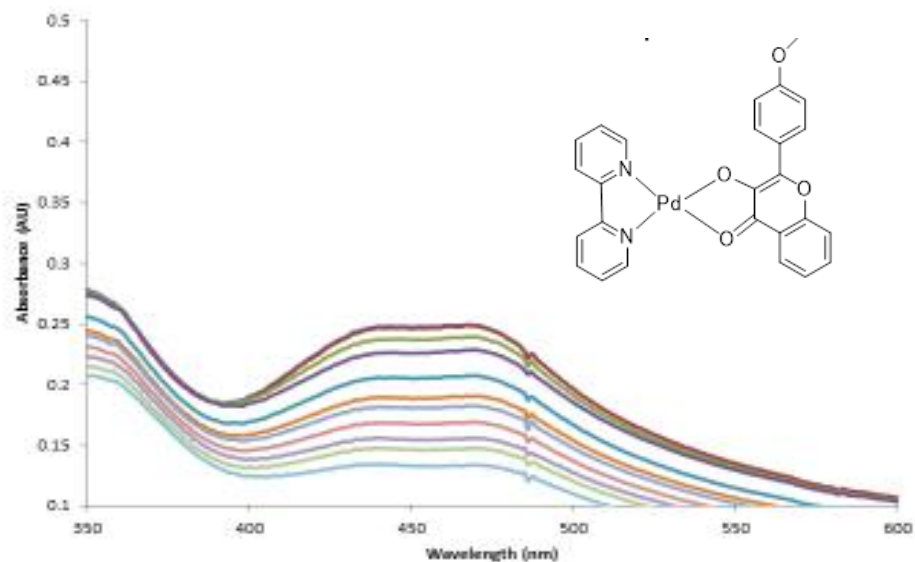


Figure 46. UV-Vis absorption spectra of reaction between complex **1** with HNO donor Angeli's salt in pH 7.1 phosphate buffer.

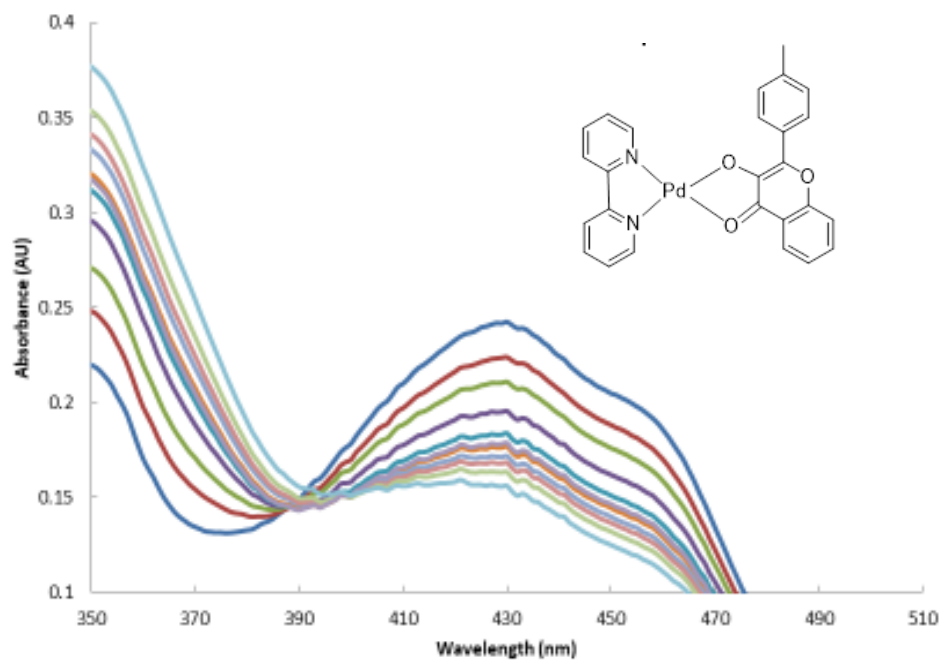


Figure 47. UV-Vis absorption spectra of reaction between complex **2** with HNO donor Angeli's salt in pH 7.1 phosphate buffer.

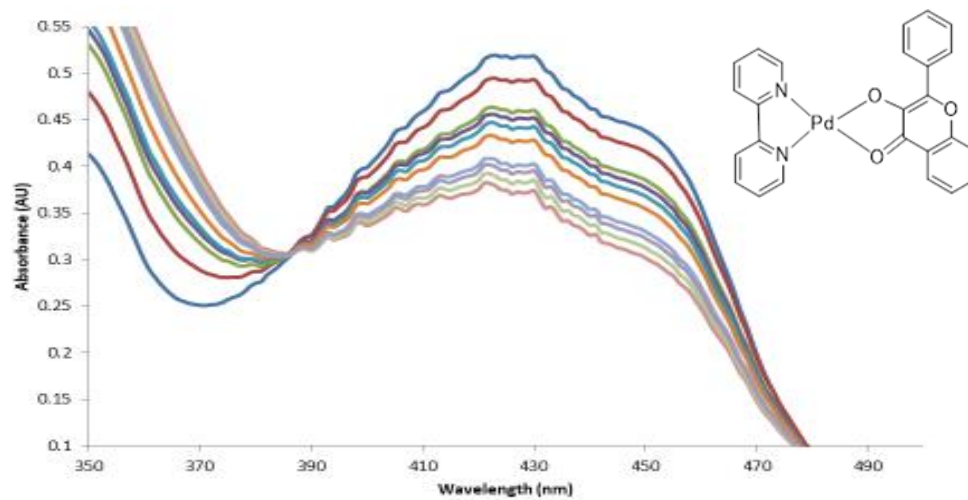


Figure 47. UV-Vis absorption spectra of reaction between complex **3** with HNO donor Angeli's salt in pH 7.1 phosphate buffer.

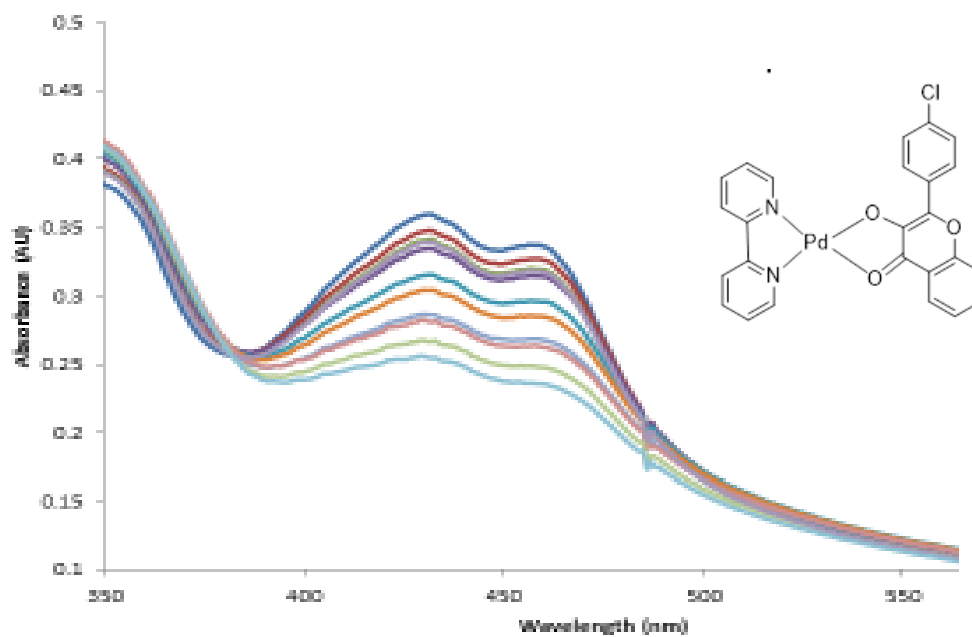


Figure 48. UV-Vis absorption spectra of reaction between complex **4** with HNO donor Angeli's salt in pH 7.1 phosphate buffer.

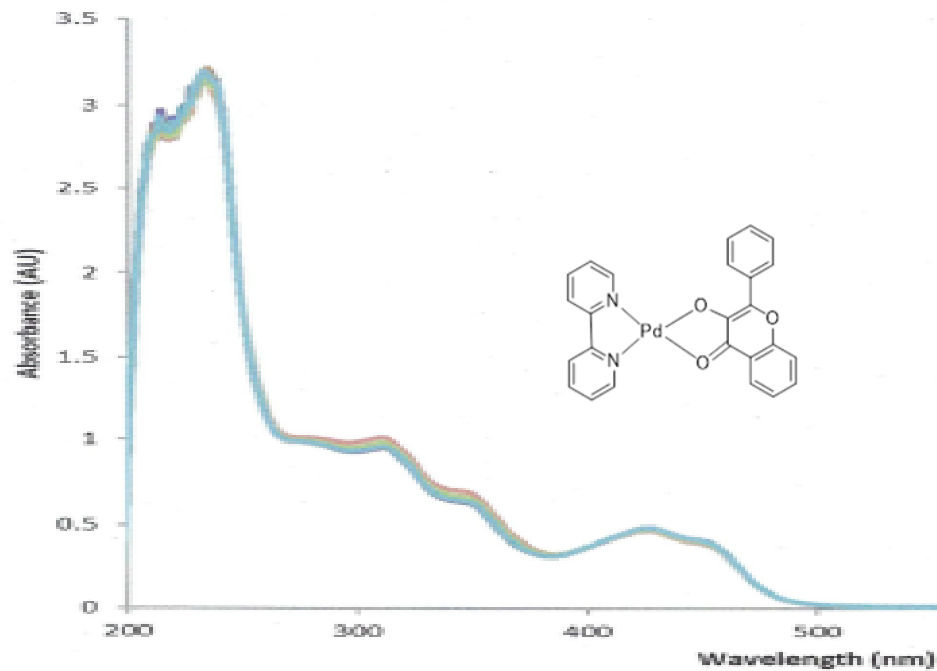


Figure 49. UV-Vis absorption spectra of reaction between complex **3** and NaNO_2 under Ar in acetonitrile.

3.8 CO detection from nitroxygenation reaction of $[\text{PdBpyFla}]\text{BF}_4$ with HNO

The product CO generated during the reaction of $[\text{PdBpyFla}]\text{BF}_4$ with HNO was confirmed by the conversion of a solution of deoxymyoglobin to its ferrous CO adduct upon exposure to the head gas above the assay mixture. Figure **51** displays the UV-Vis spectra of deoxymyoglobin and CO-myoglobin. The progress of the reaction was monitored by the shift in Soret absorbance from 434 to 423 nm, confirming formation of $\text{CO-Fe}^{\text{II}}\text{Mb}$.

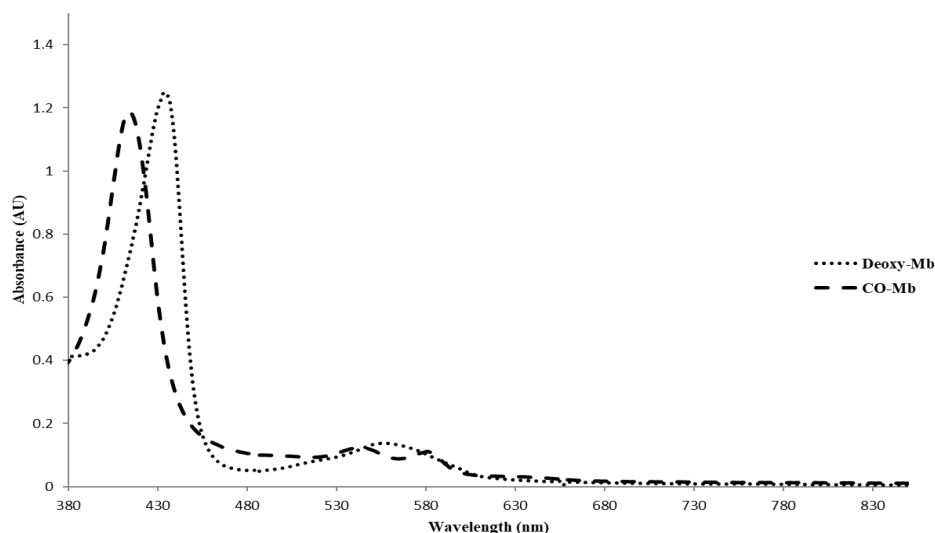
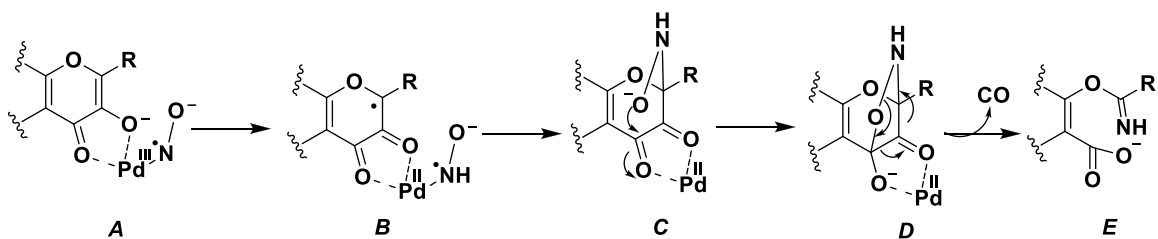
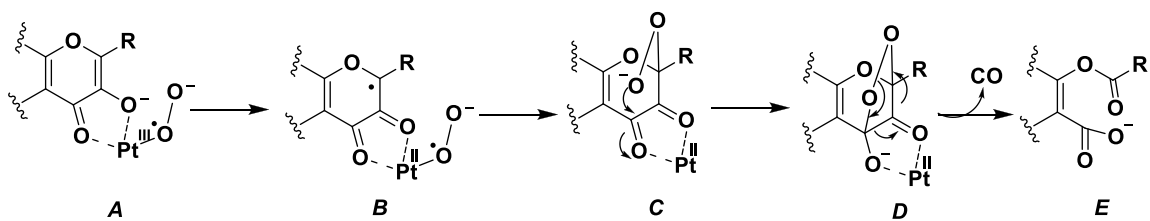


Figure 50. UV-Vis spectra of formation of CO-Fe^{II}Mb (dashed line) by deoxy-myoglobin trapping of CO released in the reaction of complex **3** with Angeli's salt.

Regarding the mechanism of nitroxygenation of metal flavonolate complex with HNO, it was reported that the metal ion acts as a conduit for an internal electron transfer between the metal-bound flavonol and HNO, also orienting the resultant organic radicals to facilitate coupling.⁵⁷ **Scheme 2** depicts possible reaction pathways for nitroxygenation activity of Pd(II) bipyridine flavonolate complexes. The reaction is proposed to go through an initial single electron transfer to form Pd^{III} – aminoxyl radical adduct, *A*. Then, a second single electron transfer from substrate to metal generates the substrate radical, *B*. Radical coupling would form an alkylhydroxamate intermediate, *C*, and then nucleophilic attack would generate an isoxazolidine bridge, *D*, which then decomposes to parent carboximidic ester, *E*, and CO. The oxygenation reaction with the Pt(II) bipyridine flavonolate complexes is likely to be similar, as depicted in **Scheme 3**.



Scheme 2. Proposed mechanism to release CO upon nitroxylation.



Scheme 3. Proposed mechanism to release CO upon oxygenation.

CHAPTER 4 - CONCLUSIONS

In summary, we designed and synthesized a series of Pd^{II} flavonolate complexes [Pd^{II}BpyFla^R] (R= *p*-OMe (**1**), *p*-Me (**2**), *p*-H (**3**) and *p*-Cl (**4**) and Pt^{II} flavonolate complexes [Pt^{II}BpyFla^R] (R = *p*-OMe (**5**), *p*-Me (**6**), and *p*-H (**7**)) as CO-releasing agents. Their structures, spectroscopic features and reaction towards dioxygen and HNO were investigated. The reaction of palladium(II) bipyridine flavonolate complexes with O₂ at room temperature with and without light irradiation doesn't occur, while their reaction with HNO at room temperature happens at a fast rate. The product CO generated from the nitroxygenation reaction of [Pd^{II}BpyFla^R] with HNO was detected by deoxymyoglobin with the shift in Soret absorbance from 434 to 423 nm. The platinum(II) bipyridine flavonolate complexes are stable in the dark but reacted with O₂ at room temperature with light irradiation to produce putative CO and an O-benzoylsalicylate product. The mechanism of nitroxygenation reaction was proposed to proceed through initial electron transfer between metal Pd^{II} and HNO. The mechanism of the platinum complexes' oxygenation reaction is probably similar with an electron transfer between Pt^{II} and O₂. The complexes' photoreactivity offers temporospatial control of CO release with potential anticancer applications. Because CO can be released at room temperature rather than requiring temperatures above body temperature, these complexes could be suitable for treatments in the human body. Since the CO release occurs only with photo-irradiation, the

CO release can be controlled, for example, to deliver small amounts of carbon monoxide selectively to cancer cells. Finally, the fact that visible light is the trigger for the CO release means the treatment would not expose a human to harmful UV light. Future work could include quantifying the CO release and testing the complexes for oxygenation reactivity in aqueous environments to mimic biologically relevant conditions. Additionally, the toxicity of the byproducts should be investigated to establish the therapeutic potential of these complexes.

REFERENCES

- (1) Lea, M. A. Flavonol Regulation in Tumor Cells. *J. Cell. Biochem.* **2015**, *116* (7), 1190–1194.
- (2) American Cancer Society. Economic Impact of Cancer <https://www.cancer.org/cancer/cancer-basics/economic-impact-of-cancer.html> (accessed Nov 29, 2018).
- (3) Zheng, W.; Zhao, Y.; Luo, Q.; Zhang, Y.; Wu, K.; Wang, F. Multi-Targeted Anticancer Agents. *Curr. Top. Med. Chem.* **2017**, *17*, 3084–3098.
- (4) Rusch, T.; Bayry, J.; Werner, J.; Shevchenko, I.; Bazhin, A. V. Immunotherapy as an Option for Cancer Treatment. *Arch. Immunol. Ther. Exp.* **2018**, *66*, 89–96.
- (5) Rosenberg, S. A. A New Era for Cancer Immunotherapy Based on the Genes That Encode Cancer Antigens. *Immunity* **1999**, *10*, 281–287.
- (6) Institute, N. C. (NIH). Organ-Related Inflammation and Immunotherapy <https://www.cancer.gov/about-cancer/treatment/side-effects/organ-inflammation> (accessed Jan 11, 2020).
- (7) Institute, N. C. New Drugs, New Side Effects - Complications of Cancer Immunotherapy <https://www.cancer.gov/news-events/cancer-currents-blog/2019/cancer-immunotherapy-investigating-side-effects> (accessed Jan 11, 2020).
- (8) Afzal, O.; Kumar, S.; Haider, M. R.; Ali, M. R.; Kumar, R.; Jaggi, M.; Bawa, S. A Review on Anticancer Potential of Bioactive Heterocycle Quinoline. *Eur. J. Med. Chem.* **2015**, *97*, 871–970.
- (9) Kurzwehnart, A.; Kandioller, W.; Bartel, C.; Bächler, S.; Trondl, R.; Mühlgassner, G.; Jakupec, M. A.; Arion, V. B.; Marko, D.; Keppler, B. K.; et al. Targeting the DNA-Topoisomerase Complex in a Double-Strike Approach with a Topoisomerase Inhibiting Moiety and Covalent DNA Binder. *Chem. Commun.* **2012**, *48* (40), 4839–4841.
- (10) Pal, M.; Nandi, U.; Mukherjee, D. Detailed Account on Activation Mechanisms of

Ruthenium Coordination Complexes and Their Role as Antineoplastic Agents. *Eur. J. Med. Chem.* 2018.

- (11) Sadler, P. J.; Noffke, A. L.; Habtemariam, A.; Pizarro, A. M. Designing Organometallic Compounds for Catalysis and Therapy. *Chem. Commun.* **2012**, *48*, 5219–5246.
- (12) Motterlini, R.; Otterbein, L. E. The Therapeutic Potential of Carbon Monoxide. *Nat. Rev.* **2010**, *9*, 728–743.
- (13) Kottelat, E.; Zobi, F. Visible Light-Activated PhotoCORMs. *Inorganics*. MDPI Multidisciplinary Digital Publishing Institute June 1, 2017.
- (14) Wegiel, B.; Gallo, D.; Csizmadia, E.; Harris, C.; Belcher, J.; Vercellotti, G. M.; Penacho, N.; Seth, P.; Sukhatme, V.; Ahmed, A.; et al. Carbon Monoxide Expedites Metabolic Exhaustion to Inhibit Tumor Growth. *Cancer Res.* **2013**, *73* (23), 7009–7021.
- (15) Vu, T. T.; Jeong, C. Y.; Nguyen, H. N.; Lee, D.; Lee, S. A.; Kim, J. H.; Hong, S. W.; Lee, H. Characterization of Brassica Napus Flavonol Synthase Involved in Flavonol Biosynthesis in Brassica Napus L. *J. Agric. Food Chem.* **2015**, *63*, 7819–7829.
- (16) Motterlini, R.; Clark, J. E.; Foresti, R.; Sarathchandra, P.; Mann, B. E.; Green, C. J. Carbon Monoxide-Releasing Molecules. *Circ. Res.* **2002**, *90*, e17–e24.
- (17) Samsonowicz, M.; Regulska, E. Spectroscopic Study of Molecular Structure, Antioxidant Activity and Biological Effects of Metal Hydroxyflavonol Complexes. *Spectrochim. Acta - Part A Mol. Biomol. Spectrosc.* **2017**, *173*, 757–771.
- (18) Grubel, K.; Rudzka, K.; Arif, A. M.; Klotz, K. L.; Halfen, J. A.; Berreau, L. M. Synthesis, Characterization, and Ligand Exchange Reactivity of a Series of First Row Divalent Metal 3-Hydroxyflavonolate Complexes. *Inorg. Chem.* **2010**, *49* (1), 82–96.
- (19) Kubanik, M.; Tu, J. K. Y.; Söhnel, T.; Hejl, M.; Jakupec, M. A.; Kandioller, W.; Keppler, B. K.; Hartinger, C. G. Expanding on the Structural Diversity of Flavone-Derived Ruthenium^{II}(η^6 -Arene) Anticancer Agents. *Metallodrugs* **2016**, *1*, 24–35.
- (20) Yasarawan, N.; Thipyapng, K.; Ruangpornvisuti, V. Chelation Behavior of Various Flavonols and Transfer of Flanonol-Chelated Zinc (II)... *J Mol. Struct.*

2016, 1107, 278–290.

- (21) Din, M. I.; Ali, F.; Intisar, A. Metal Based Drugs and Chelating Agents as Therapeutic Agents and Their Antimicrobial Activity. *Rev. Roum. Chim.* **2019**, 64 (1), 5–17.
- (22) Selvaraj, S.; Krishnaswamy, S.; Devashya, V.; Sethuraman, S.; Krishnan, U. M. Flavonoid-Metal Ion Complexes: A Novel Class of Therapeutic Agents. *Med. Res. Rev.* **2014**, 34 (4), 677–702.
- (23) Kurzwernhart, A.; Kandioller, W.; Enyedy, É. A.; Novak, M.; Jakupec, M. A.; Keppler, B. K.; Hartinger, C. G. 3-Hydroxyflavones vs. 3-Hydroxyquinolinones: Structure-Activity Relationships and Stability Studies on Ru^{II}(Arene) Anticancer Complexes with Biologically Active Ligands. *Dalt. Trans.* **2013**, 42, 6193–6202.
- (24) Baranovic, G.; Segota, S. Infrared Spectroscopy of Flavones and Flavonols. Reexamination of the Hydroxyl and Carbonyl Vibrations in Relation to the Interactions of Flavonoids with Membrane Lipids. *Spectrochim. Acta Part A Mol. Biomol. Spectrosc.* **2018**, 192, 473–486.
- (25) Kurzwernhart, A.; Mokesch, S.; Klapproth, E.; Adib-Ravazi, M. S.; Jakupec, M. A.; Hartinger, C. G.; Kandioller, W.; Keppler, B. K. Flavonoid-Based Organometallics with Different Metal Centers - Investigations of the Effects on Reactivity and Cytotoxicity. *Eur. J. Inorg. Chem.* **2016**, 2016 (2), 240–246.
- (26) Benavente-García, O.; Castillo, J. Update on Uses and Properties of Citrus Flavonoids: New Findings in Anticancer, Cardiovascular, and Anti-Inflammatory Activity. *J. Agric. Food Chem.* **2008**, 56, 6185–6205.
- (27) Li, X.; Chen, G.; Zhang, X.; Zhang, Q.; Zheng, S.; Wang, G.; Chen, Q. H. A New Class of Flavonol-Based Anti-Prostate Cancer Agents: Design, Synthesis, and Evaluation in Cell Models. *Bioorganic Med. Chem. Lett.* **2016**, 26 (17), 4241–4245.
- (28) Britton, R. G.; Horner-Glister, E.; Pomenya, O. A.; Smith, E. E.; Denton, R.; Jenkins, P. R.; Steward, W. P.; Brown, K.; Gescher, A.; Sale, S. Synthesis and Biological Evaluation of Novel Flavonols as Potential Anti-Prostate Cancer Agents. *Eur. J. Med. Chem.* **2012**, 54, 952–958.
- (29) Saraf, S. L.; Fish, T. J.; Benninghoff, A. D.; Buelt, A. A.; Smith, R. C.; Berreau, L. M. Photochemical Reactivity of Ru^{II}(η^6 -*p*-Cymene) Flavonolato Compounds.

Organometallics **2014**, *33*, 6341–6351.

- (30) Movassaghi, S.; Leung, E.; Hanif, M.; Lee, B. Y. T.; Holtkamp, H. U.; Tu, J. K. Y.; Söhnel, T.; Jamieson, S. M. F.; Hartinger, C. G. A Bioactive L-Phenylalanine-Derived Arene in Multitargeted Organoruthenium Compounds: Impact on the Antiproliferative Activity and Mode of Action. *Inorg. Chem.* **2018**, *57*, 8521–8529.
- (31) Popova, M.; Soboleva, T.; Ayad, S.; Benninghoff, A. D.; Berreau, L. M. A Visible Light-Activated Quinolone Carbon Monoxide-Releasing Molecule: Prodrug and Albumin-Assisted Delivery Enable Anti-Cancer and Potent Anti-Inflammatory Effects. *J. Am. Chem. Soc.* **2018**, *140*, 9721–9729.
- (32) Soboleva, T.; Esquer, H. J.; Benninghoff, A. D.; Berreau, L. M. Sense and Release: A Thiol-Responsive Flavonol-Based Photonically Driven Carbon Monoxide-Releasing Molecule That Operates via a Multiple-Input AND Logic Gate. *J. Am. Chem. Soc.* **2017**, *139* (28), 9435–9438.
- (33) Han, X.; Kumar, M. R.; Hoogerbrugge, A.; Klausmeyer, K. K.; Ghimire, M. M.; Harris, L. M.; Omary, M. A.; Farmer, P. J. Mechanistic Investigations of Photoinduced Oxygenation of Ru(II) Bis-Bipyridyl Flavonolate Complexes. *Inorg. Chem.* **2018**, *57*, 2416–2424.
- (34) Hanif, M.; Hartinger, C. G. Organometallics in Cancer Treatment--Non-Conventional Structures and Modes of Action. In *Reference Module in Chemistry, Molecular Sciences and Chemical Engineering.*; Reedjik, J., Ed.; 2018; pp 1–9.
- (35) Kumar, R.; Shin, W. S.; Sunwoo, K.; Kim, W. Y.; Koo, S.; Bhuniya, S.; Kim, J. S. Small Conjugate-Based Theranostic Agents: An Encouraging Approach for Cancer Therapy. *Chem. Soc. Rev.* **2015**, *44* (19), 6670–6683.
- (36) Siegbahn, P. E. M. Hybrid DFT Study of the Mechanism of Quercetin 2,3-Dioxygenase. *Inorg. Chem.* **2004**, *43*, 5944–5953.
- (37) Balogh-Hergovich, É.; Speier, G. Kinetics and Mechanism of the Base-Catalyzed Oxygenation of Flavonol in DMSO-H₂O Solution. *J. Org. Chem.* **2001**, *66*, 7974–7978.
- (38) Hartinger, C. G.; Metzler-Nolte, N.; Dyson, P. J. Challenges and Opportunities in the Development of Organometallic Anticancer Drugs. *Organometallics* **2012**, *31* (16), 5677–5685.

- (39) Kurzwehnhart, A.; Kandioller, W.; Bächler, S.; Bartel, C.; Martic, S.; Buczkowska, M.; Mühlgassner, G.; Jakupec, M. A.; Kraatz, H. B.; Bednarski, P. J.; et al. Structure-Activity Relationships of Targeted Ru^{II}(η^6 -*p*-Cymene) Anticancer Complexes with Flavonol-Derived Ligands. *J. Med. Chem.* **2012**, *55*, 10512–10522.
- (40) Atkin, A. J.; Lynam, J. M.; Moulton, B. E.; Sawle, P.; Motterlini, R.; Boyle, N. M.; Pryce, M. T.; Fairlamb, I. J. S. Modification of the Deoxy-Myoglobin/Carbonmonoxy-Myoglobin UV-Vis Assay for Reliable Determination of CO-Release Rates from Organometallic Carbonyl Complexes. *Dalt. Trans.* **2011**, *40* (21), 5755–5761.
- (41) Zapata, A. L.; Kumar, M. R.; Pervitsky, D.; Farmer, P. J. A Singular Value Decomposition Approach for Kinetic Analysis of Reactions of HNO with Myoglobin. *J. Inorg. Biochem.* **2013**, *118*, 171–178.
- (42) McDaniel, D. H.; Brown, H. C. An Extended Table of Hammett Substituent Constants Based on the Ionization of Substituted Benzoic Acids. *J. Org. Chem.* **1958**, *23* (3), 420–427.
- (43) Kaizer, J., Baráth, G., Pap, J., Speier, G., Giorgi, M., & Réglér, M. Manganese and Iron Flavonolates as Flavonol 2,4-Dioxygenase Mimics. *Chem. Commun.* **2007**, *48*, 5235–5237.
- (44) Barhács, L.; Kaizer, J.; Speier, G. Kinetics and Mechanism of the Stoichiometric Oxygenation of the Ionic Zinc(II) Flavonolate Complex [Zn(Fla)(Idpa)]ClO₄ (Fla=flavonolate; Idpa=3,3'-Iminobis(N,N-Dimethylpropylamine)). *J. Mol. Catal. A Chem.* **2001**, *172* (1–2), 117–125.
- (45) Sun, Y. J.; Huang, Q. Q.; Zhang, J. J. Series of Structural and Functional Models for the ES (Enzyme-Substrate) Complex of the Co(II)-Containing Quercetin 2,3-Dioxygenase. *Inorg. Chem.* **2014**, *53* (6), 2932–2942.
- (46) Matuz, A.; Giorgi, M.; Speier, G.; Kaizer, J. Structural and Functional Comparison of Manganese-, Iron-, Cobalt-, Nickel-, and Copper-Containing Biomimic Quercetinase Models. *Polyhedron* **2013**, *63*, 41–49.
- (47) Balogh-Hergovich, É.; Kaizer, J.; Speier, G.; Fülöp, V.; Párkányi, L. Quercetin 2,3-Dioxygenase Mimicking Ring Cleavage of the Flavonolate Ligand Assisted by Copper. Synthesis and Characterization of Copper(I) Complexes [Cu(PPh₃)₂(Fla)]

- (Fla = Flavonolate) and [Cu(PPh₃)₂(O-Bs)] (O-Bs = O-Benzoylsalicylate). *Inorg. Chem.* **1999**, *38* (17), 3787–3795.
- (48) Grubel K, Laughlin BJ, Maltais TR, Smith RC, Arif AM, B. L. Photochemically-Induced Dioxygenase-Type CO-Release Reactivity of Group 12 Metal Flavonolate Complexes. *Chem Commun* **2011**, *47* (37), 10431–10433.
- (49) Kaizer, J.; Pap, J.; Speier, G.; Párkányi, L. The Reaction of μ - η^2 : η^2 -Peroxo- and Bis(μ -oxo)Dicopper Complexes with Flavonol. *Eur. J. Inorg. Chem.* **2004**, *11*, 2253–2259.
- (50) Balogh-Hergovich, E., Kaizer, J., Pap, J., Speier, G., Huttner, G., & Zsolnai, L. Copper-Mediated Oxygenolysis of Flavonols via Endoperoxide and Dioxetan Intermediates. *Eur. J. Inorg. Chem.* **2002**, *9*, 2287–2295.
- (51) Sun, Y. J.; Huang, Q. Q.; Tano, T.; Itoh, S. Flavonolate Complexes of M^{II} (M = Mn, Fe, Co, Ni, Cu, and Zn). Structural and Functional Models for the ES (Enzyme-Substrate) Complex of Quercetin 2,3-Dioxygenase. *Inorg. Chem.* **2013**, *52* (19), 10936–10948.
- (52) Lippai, I.; Speier, G. Quercetinase Model Studies. The Oxygenation of Flavonol Catalyzed by a Cationic 2,2'-Bipyridine Copper(II) Flavonolate Complex. *J. Mol. Catal. A Chem.* **1998**, *130* (1–2), 139–148.
- (53) Barhács, L.; Kaizer, J.; Speier, G. Kinetics and Mechanism of the Oxygenation of Potassium Flavonolate. Evidence for an Electron Transfer Mechanism. *J. Org. Chem.* **2000**, *65* (11), 3449–3452.
- (54) Pap JS, Matuz A, Baráth G, Kripli B, Giorgi M, Speier G, K. J. Bio-Inspired Flavonol and Quinolone Dioxygenation by a Non-Heme Iron Catalyst Modeling the Action of Flavonol and 3-Hydroxy-4(1H)-Quinolone 2,4-Dioxygenases. *J Inorg Biochem.* **2012**, *108*, 15–21.
- (55) Soboleva, T.; Berreau, L. M. 3-Hydroxyflavones and 3-Hydroxy-4-Oxoquinolines as Carbon Monoxide-Releasing Molecules. *Molecules* **2019**, *24*, 1252.
- (56) Al-afyouni, M. H.; Rohrabough, T. N.; Al-afyouni, K. F.; Turro, C. New Ru(II) Photocages Operative with near-IR Light: New Platform for Drug Delivery in the PDT Window. *Chem.Sci.* **2018**, *9*, 6711–6720.
- (57) Kumar, M. R.; Zapata, A.; Ramirez, A. J.; Bowen, S. K.; Francisco, W. A.;

Farmer, P. J. Nitrosyl Hydride (HNO) Replaces Dioxygen in Nitroxygenase Activity of Manganese Quercetin Dioxygenase. *Proc. Natl. Acad. Sci.* **2011**, *108* (47), 18926–18931.

- (58) Han, X.; Kumar, M. R.; Farmer, P. J. Nitroxygenation of Quercetin by HNO. *Tetrahedron Lett.* **2016**, *57* (3), 399–402.

